

The Determinants of Decadal Methane Lifetime Change in the Chemistry Climate Model SOCOL: 1900 – 2000

Presented by:

Dogushan Kilic

October 2012

Supervisor:

Prof. Stefan Brönnimann

Co-Supervisor:

Prof. Thomas Peter

Geography Institute of the University of Bern
Oeschger Centre for Climate Change Research, University of Bern

ABSTRACT

During the 20th century, the atmospheric methane mixing ratio has increased substantially, albeit with varying growth rates. While the growth rate increased until the 1970s, in recent decades it has exhibited a declining trend. The goal of this study is to analyze the extent to which the changes in methane lifetime are due to changes in the strength of atmospheric methane sinks.

Simulations using the Chemistry Climate Model Solar Climate Ozone Links (SOCOL) v2.0 are analyzed over the period 1900 to 1999. Transient boundary conditions, including sea-surface temperatures, greenhouse gases, and land-surface conditions, were included in the model. In SOCOL, methane is not emitted; rather concentrations are prescribed according to observations. In this thesis, methane destruction rates are analyzed, allowing conclusions to be drawn regarding changes in methane lifetime. In the model, methane lifetime increased in the 1900-1960 period (from 6.8 to 7.2 years), then decreased from the late 1960s until the end of the 20th century (from 7.2 to 7 years). This analysis shows that the increase in methane lifetime from 1900 to 1960 is related to a reduction in tropospheric OH levels which is caused by an increase in the methane mixing ratio. It also demonstrates that the decrease in methane lifetime after 1960 is a consequence of the recovery of OH in troposphere which is caused by increases in NO_x emissions which results in enhanced ozone formation. Therefore, this study proposes that a NO_x induced methane oxidation mechanism over the continental troposphere causes changes in methane lifetime and its growth rate in the long-term.

1. INTRODUCTION

Methane (CH₄) is the most important greenhouse gas (GHG) after carbon dioxide (CO₂) in terms of its radiative forcing (IPCC, 2007). At the same time it is an abundant reactive gas that plays a key role in various chemical reactions in the atmosphere such as ozone formation. Methane, together with ozone and aerosols, is therefore, one of the most important agents in chemistry-climate interactions. For this reason, understanding the factors that alter the lifetime of atmospheric methane and affect its growth rate is particularly important for future climate research, since a profound change in its lifetime has the potential to significantly affect the global climate.

Atmospheric methane concentrations have exhibited an increasing trend in 20th century. The mixing ratio was 1774 ppb in 2005 and increased by 1059 ppb since pre-industrial times (IPCC, 2007). While the strength of each source is not very well known, the increase in the CH₄ mixing ratio could be caused by both anthropogenic and natural emissions (Forster et al., 2007). Natural sources include natural wetlands, wildfires, and geological processes, and the anthropogenic sources include flooded rice fields (Neue, 1993), landfills, waste treatment facilities, natural gas handling, biomass burning, and fossil fuel combustion (EPA, 2010). Any shift in the emission trends of CH₄, raises concerns related to their impact on the climate since methane is a much more potent greenhouse gas than CO₂ on a per molecule basis.

The methane growth rate has decreased over the 1984-1996 period and this rate exhibits significant inter-annual variability (Dlugokencky et al., 1998; 2001). The causes of this declining growth rate have puzzled many scientists. Studies have proposed either reductions in methane emissions (Karlsdottir and Isaksen, 2000), due to reduced fossil fuel emissions (Aydin et al., 2011) and biogenic emissions (Kai et al., 2011), or changes in sink mechanisms (Fiore et al., 2006) as the primary explanations for this trend.

In this study we focus on decadal changes in atmospheric methane sinks as a determinant of methane lifetime and growth rates. The variability in methane lifetime in the 20th century is investigated using simulations of the coupled chemistry-climate model (CCM) SOCOL. Methane concentrations are prescribed in the CCM-SOCOL. Thus, the same methane mixing ratio is defined in the lowest model layer globally and transported through to the upper atmosphere.

1.1. Objectives

The aim of this Master's thesis is to better understand the drivers that affect methane lifetime and the mechanisms responsible for the land-sea contrast in methane sinks. This thesis will demonstrate that the decadal change in methane lifetime could be explained by either rising temperatures, as a consequence of climate change, or the variability of OH levels due to changes in their associated sink or source mechanisms.

First, methane sinks are expected to be enhanced due to an increase in the temperature dependent "CH₄ + OH" reaction rate which is caused by rising tropospheric temperatures. These rising tropospheric temperatures may also explain the land-sea contrast in methane sinks as this temperature effect may vary due to the diurnal variation over land and marine bodies.

Second, assuming that the long-term variability of OH sinks is caused by a long-term change in methane lifetime, one could expect that OH sinks were initially enhanced until the 1970s, at which point this enhancement stopped and receded in last 30 years of the 20th century. In this case, the trends of major OH sinks in the target period are expected to exhibit a similar pattern to that related to methane lifetime.

Finally, the change in OH sources may be the cause of changes in decadal methane lifetimes, therefore a reduction in OH concentrations until 1970 is expected. Then, due to changes in OH sources, OH levels increase globally creating an opposing impact on methane lifetime. In both cases, due to the changing OH levels, we also expect to see changes in the land-sea contrast of the methane sink.

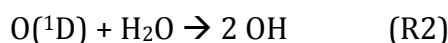
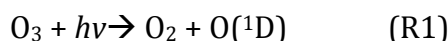
The analysis will allow us to understand whether increasing tropospheric temperatures, OH sinks or sources, are responsible for the decadal methane lifetime change. The CCM SOCOL simulations, sensitivity runs and calculations will enable the quantification and the monitoring of the effects.

2. BACKGROUND

2.1. Methane Chemistry in Troposphere

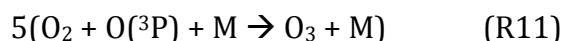
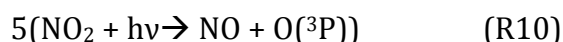
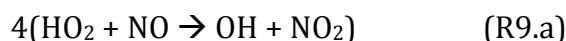
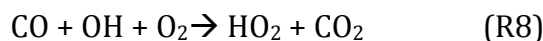
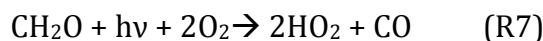
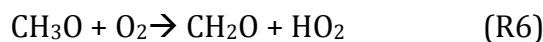
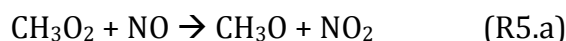
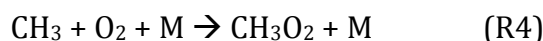
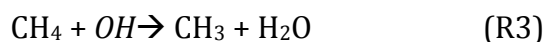
The primary sink of methane occurs through its reaction with the hydroxyl radical (OH) (Johnson et al., 2002). Smaller amounts of methane may be removed through other sinks such as its absorption by soils (Born et al., 1990), transport to the stratosphere where methane is removed by OH, Cl and O(¹D), and reaction with Cl in the Planetary Boundary Layer(PBL) (Platt et al., 2004; Allan et al., 2005). Some of these minor sinks are not included in the model of the atmosphere used here e.g. absorption by soils. These minor sinks account for approximately 10% of the total loss of tropospheric methane (Fung et al., 1991; Hein et al., 1997;Lelieveld et al., 1998). Hence, in this model, approximately 90% of global tropospheric methane is oxidized by OH. Therefore, methane loss is primarily determined by atmospheric OH and its temporal change.

Because OH is the dominant methane sink , OH density is an important consideration in this study. Most OH is produced through the reaction of O(¹D) with water vapor (R1) in the lower troposphere (Chen et al., 2001).



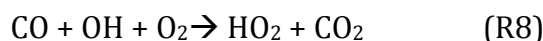
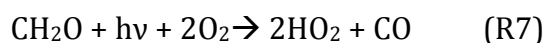
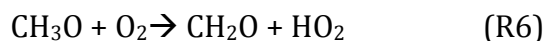
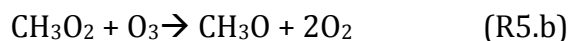
Ozone (O₃), being a collateral source of methane oxidizing OH, is photochemically destroyed (R1) (Penkett et al., 1994). The photolysis of O₃, forming O(¹D) as one of its products, occurs at wavelengths shorter than 340 nm. If the increase in UV-B (280 – 315 nm) radiation in the troposphere (Brönnimann et al., 2001) due to stratospheric ozone depletion (WMO, 2006) is considered, the production of OH could be enhanced by an elevated R1 rate.

Another important mechanism that affects methane lifetime is enhanced ozone formation, leading to increases in OH levels by ozone photolysis in industrialized regions with high levels of air pollution (Whalley et al., 2010). The enhanced methane oxidation, as a result of enhanced OH formation due to rising ozone levels, may increase the OH mixing ratio by increasing tropospheric ozone levels. This mechanism, following R1, is formulated as:



Ozone, following the pathways in R1 and R2, produces additional O(¹D) over land by photolysis where the mixing of NO_x is higher. Thus, the elevated O(¹D) leads to increased OH levels and methane lifetime is decreased by repeating the methane oxidation cycle given from R1 to R11.

On the other hand the methane oxidation mechanism has different avoided NO_x conditions, for example in the troposphere over the mid-ocean. This process following R1-R4 is as follows:



In NO_x avoided regions such as in the marine troposphere, ozone is used for the oxidation of methane (R5.b and R9.b). In these regions, because there is no surface-NO_x source for ozone formation, ozone is transported either from the stratosphere or neighboring land masses. Ozone formation is thus lower than in continental areas in these regions. As a result, the mixing ratio of OH is lower compared to NO_x-rich

continental regions, due to a lack of tropospheric ozone. Methane oxidation by OH is also not as efficient as it is on land, due to lower OH levels.

There are other species, such as NO_x and Volatile Organic Compounds (VOCs), which are oxidized by OH as well. VOCs are not part of the atmospheric chemistry modeled in CCM SOCOL, however, any change in the removal of OH by NO₂ would affect OH levels. As a result, the removal of OH by NO₂ affects methane lifetime as a competitive agent. In this study changes in the regional and global HNO₃ concentrations, which are dependent on the “NO₂ + OH” reaction, are also investigated in order to analyze the direction of the OH sink impact on methane lifetime.

2.2. ENSO, Temperature, Water Vapor and, Methane Lifetime

Khalil and Rasmussen (1986) postulated that the inter-annual variation of methane measurements at Cape Meares (45°N, 124°W) is linked with El Nino Southern Oscillation (ENSO) events which enhance the removal of methane through higher concentrations of water vapor, which result in a greater abundance of OH. Bekki and Law (1997), using a 2-D global atmospheric chemistry model, explored the OH changes resulting from variability in tropospheric temperatures. They found that these changes could also cause variations in methane growth rates of a few ppb per year. Therefore, the rate of methane oxidation may be influenced by an increase in temperature and humidity due to climate change (Johnson et al., 1999; 2001; Stevenson et al., 2000).

El Nino (La Nina) is characterized by monthly mean SST anomalies in the Nino 3.4 region bounded by 120°W – 170°W and 5°S – 5°N, that is + 0.5°C (- 0.5°C) higher (lower) than the all times mean using the Oceanic Nino Index (Trenberth K.E., 1997). In this study, analysis focusing on the ENSO region is bounded by the same boundaries.

3. METHODS

3.1. Chemistry Climate Model SOCOL(CCM-SOCOL)

The CCM SOCOL version 2.0 (Schraner et al., 2008) is a combination of the middle atmosphere version of the general circulation model (GCM) MA-ECHAM4 (Roeckner et al., 1996; Manzini and Bengtsson, 1996) and a modified version of the chemistry-transport model MEZON (Model for Evaluation of oZONe trends) (Rozañov et al., 1999, 2001; Egorova et al., 2001, 2003; Hoyle, 2005). MA-ECHAM4 has a grid spacing of 3.75° with T30 horizontal truncation, and 39 vertical levels in a hybrid sigma-pressure coordinate system covering the model atmosphere from surface to 0.01 hPa. The time step for the dynamic processes and physical process parameterizations in MA-ECHAM is 15 minutes. The time step for full radiative transfer calculations is 2 hours where heating and cooling rates are interpolated for every 15 minute period. The chemistry component of the CCM SOCOL simulates 41 chemical species from the oxygen, hydrogen, nitrogen, carbon, chlorine and bromine groups, driven by 118 gas-phase reactions, 33 photolysis reactions and 16 heterogeneous reactions on sulphate aerosols and polar stratospheric clouds.

Some abilities of the CCM-SOCOL version 2.0 are limited with respect to both climate and chemistry simulations. Starting with its GCM component, MA-ECHAM4, belongs to an older generation of GCMs. There is increased spectral resolution of shortwave radiation parameterization in MA-ECHAM5 in the UV-B and UV-C bands. This is accomplished by improving the parameterization of shortwave fluxes and heating rates (Cagnazzo et al., 2006).

The absence of VOCs in the model also affects the reliability of the atmospheric chemistry in the model. The variability of OH is partly hindered due to the lack of VOCs in the model because VOCs could enhance the formation of ozone, as an OH source, and buffer OH (Taraborelliet al., 2012). Similarly, the absence of prescribed methane concentrations that vary annually, implies that the variability of methane emissions due to other actors such as climate are also omitted from the model.

Another important element to note is the failure of the model to include the impact of clouds on ozone photolysis. Clouds are parameterized in the model, none-the-less, the ozone photolysis rate (UV radiation for $O(^1D)$ formation) is independent of clouds. As a result, the altitude of clouds and cloud intensity do not affect UVB radiation intensity,

which is important for O(¹D) formation (R1). However, despite these short-comings, the CCM-SOCOL is appropriate to study the key drivers of methane lifetime and to test our hypothesis targeting methane sink mechanism(s).

3.1.1. Boundary Conditions

In the SOCOL model, atmosphere, solar irradiance, greenhouse gases (GHGs), NO_x and CO emissions, ozone depleting substances (ODSs), tropospheric aerosols, sea surface temperature, sea ice, land surface change, quasi-biennial oscillations and stratospheric aerosols have versatile temporal and spatial variability (Fischer et al., 2008). The simulations carried out with the CCM SOCOL analyzed in this study, cover the 20th century from 1901 to 1999.

GHGs (CO₂, N₂O, CH₄ and CFCs) (Etheridge et al., 1996) and ODSs (WMO, 2003) have globally constant values that vary annually. Surface CO and NO_x emissions (Schultz et al., 2007; van Aardenne et al., 2001) have spatial, 1°x1° resolution in the 1900-1960 period and 0.5°x0.5° resolution after 1960, both vary monthly. Monthly aircraft NO_x emissions are latitude and altitude dependent, and are included in the modeled atmosphere of the SOCOL model starting in 1960 (Schmitt et al., 1997).

Hadley Center's HadISST (Rayner et al., 2003) dataset is used for sea ice and sea surface temperature simulations. Both parameters vary monthly and have a spatial resolution of 1°x 1°. This data set is available from 1870 to today.

The land surface change is simulated by HYDE data containing 20 vegetation classes in the CCM-SOCOL (Goldewijk K.K., 2001). From 1700 to 1950 land surface change is updated on a 50-year interval, additionally for 1970 and 1990.

All input data is regridded to the model's horizontal resolution and further detail on the input data is available on the SOCOL-website¹ including information on quasi-biennial oscillation, tropospheric and stratospheric aerosols.

3.1.2. Sensitivity Runs and Calculations

Ordinarily a sensitivity analysis would imply keeping all parameters except for one constant and monitoring the resulting variation in all (calculated) variables. Mathematically, this corresponds to a "variation", which is equal to the partial derivative of the variables in the case where these variables are linearly dependent.

¹ Available on: <http://www.iac.ethz.ch/en/research/socol/data.htm>

In this study two sensitivity runs are analyzed in which the test parameters were CH₄, CO and NO_x. In a “fixed methane” run, CH₄_1901, the CH₄ mixing ratio is kept constant at 1901 levels where all other trace gases such as GHGs, ODPs, NO_x and CO vary monthly in all years. In another sensitivity run, NO_x_CO_1951, CO and NO_x levels are stabilized at 1951 levels, with all others varying.

Our analysis presents the findings of all three runs –all parameters varying, fixed methane, and fixed CO and NO_x–for the 20th century concerning CH₄ lifetime.

Table 3.1 Boundary conditions of CCM SOCOL runs in the study

Experiment name	Simulation period	Description
REF	1901 - 2000	Boundary conditions as described in section 3.1.1
CH ₄ _1901	1901 - 2000	CH ₄ boundary condition fixed to 1901, all other boundary conditions according to REF
NO _x _CO_1951	1951 – 2000	NO _x and CO emissions fixed to 1951, all other boundary conditions according to REF

The total calculated lifetime of atmospheric methane (τ_{CH_4}) can be given by the equation:

$$\tau_{\text{CH}_4} = \frac{\text{total CH}_4}{\text{total CH}_4 \text{ destruction}}$$

“Total CH₄” and “total CH₄ destruction” in equation 1 represent the sum of the methane number densities (molecules/cm³) times their associated grid volumes and the rates of total methane oxidation by OH, Cl and O(1D) (molecules/sec) of all grids, respectively. Using the methane mixing ratios prescribed in the model, number densities are calculated for each grid cell according to the grid temperature and pressure.

Total methane destruction is calculated for each grid cell as the sum of “CH₄ + OH → CH₃ + H₂O”, “CH₄ + CL → CH₃ + HCl” and “CH₄ + O(1D) → CH₃ + OH” rates. Rates such as

temperature, pressure, ozone, H₂O, OH, HO₂, NO_x, HNO₃, methane and Cl are written in the model output data on a monthly basis for the 20th century. The monthly mean O(¹D) mixing ratios, where OH is determined with H₂O (R2), are not written in the model output. Using the ozone volume density and photolysis rates, monthly mean O(¹D) number densities are, however, calculated for each grid cell.

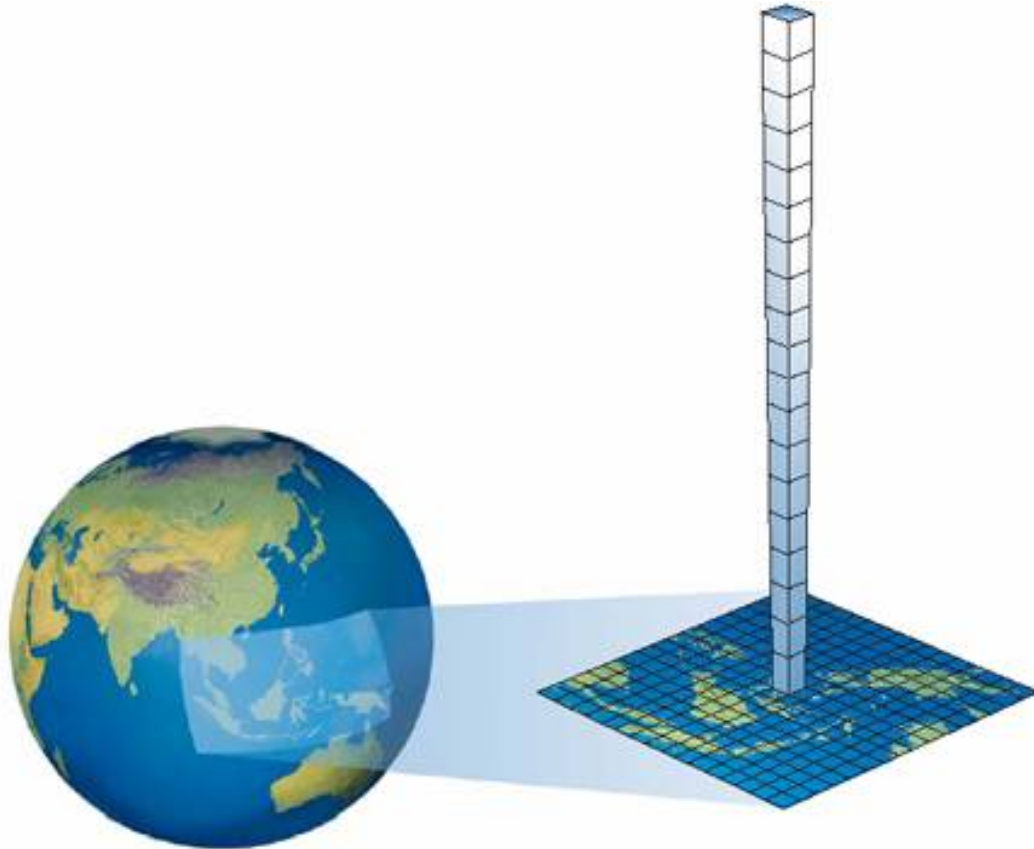


Figure 3.1 The scheme shows how the areal average of the grids is calculated. The values of each grid cell at the same pressure level are weighted by grid cross-section area, which vary with latitude and longitude. The mean values of each pressure layer are also weighted by grid height for atmospheric temperature and by density for trace gases in order to calculate tropospheric and global mean values.²

The grid pressure values written in the model output vary from 1000 hPa to 0.01 hPa. In addition to vertical pressure layers, the grid center values vary with time (monthly), latitude (50) and longitude (96). In order to calculate grid box height, the mean of the two consequent pressure levels are used. The grid height is calculated from the pressure difference in this manner. Grid area is calculated for each grid box depending on the grid location (latitude/longitude). Following the calculation of grid volume and molecular densities of the trace gases at each grid cell, the weighted areal mean of all grids at the

² Source: http://www.climateprediction.net/science/sci_images/PRECIS_resolution.jpg

same pressure level is calculated (figure 3.1). The areal weighted average is used to obtain one weighted-mean value for vertical pressures from 1000 hPa to 0.01 hPa. Finally, Tropospheric mean values are calculated by weighting vertical level means by density (molecular density and volume mixing ratio) from 1000 – 250 hPa and from 1000 – 0.01 hPa for the atmosphere.

Grid cells below the topography are also considered in tropospheric and atmospheric mean estimates. The values of modeled grid cells located in a mountain are imaginary. These grids are not normally part of the atmosphere. By comparing the grid pressure with the upper adjacent grid pressure, the weight of the value is given as “0”. To this end the mean value of the grid cell which is normally covered by topography is omitted in the tropospheric or atmospheric mean calculations.

Averaging the OH molecular density for comparison with previous studies is done using the same method used to calculate the tropospheric and atmospheric means. However, because previous studies have mean estimates below 100 hPa, vertical layer boundaries are 1000 – 100 hPa.

In addition to the global mean methane destruction analysis, this study focuses on selected terrestrial and marine regions. These regions are selected due to their varying atmospheric properties. Europe is selected due to its pollution levels, i.e. it is NO_x abundant; the Sahara is selected because it has a NO_x poor troposphere; and the ENSO 3.4 region is selected because tropospheric temperatures could be elevated for longer periods (3 - 5 months) from the surface to the top of the troposphere. The borders of the selected regions are given in table 3.2.

Table 3.2 Borders of the selected regions where methane destruction by OH analyzed

Region	Borders (Longitude / Latitude)
EUROPE	40°N – 60°N / 10°W – 40°E
ENSO 3.4	120°W – 170°W / 5°S – 5°N
SAHARA	14°N – 30°N / 10°W – 30°E

Over the regions of interest, the variability in methane destruction rates caused by OH is analyzed via sensitivity calculations. First, the global mean trend of the “CH₄ + OH” rate in the 20th century is calculated via monthly rates written in the model output. Then, using monthly mean temperatures, molecular densities of CH₄ and OH destruction rates

are calculated according to the scenarios given in the table 3.3, in order to quantify the impact of all actors on methane lifetime: methane, OH and temperature.

Table 3.3 Description of the “CH₄ + OH” rate sensitivity calculations in the study

Calculation name	Calculation period	Description
REF	1901 – 2000	“CH ₄ + OH” rate written in the model output data. CH ₄ , OH and temperature vary according to REF
FX_CH4	1901 – 2000	“CH ₄ + OH” rate calculated for the CH ₄ boundary condition fixed to 1901. OH and temperature vary according to REF
FX_OH	1901 – 2000	“CH ₄ + OH” rate calculated for the OH boundary condition fixed to 1901. CH ₄ and temperature vary according to REF
FX_Temp	1901 – 2000	“CH ₄ + OH” rate calculated for the temperature boundary condition fixed to 1901. CH ₄ and OH vary according to REF

4. RESULTS and DISCUSSION

Methane sinks increased globally in the 20th century as did its mixing ratio. In the CCM-SOCOL, total global methane sinks amount to around 350 Tg annually at the beginning of the model period and rise to 650-700 Tg by the end of the century. This increase in sinks is enhanced in the last 40 years of the model period and its rise is steeper in that period (figure 4.1).

Methane lifetime also increases by 0.6 per year in the first 70 years of the model period. This increase then stops and the lifetime of methane starts to decrease in the last 30 years (figure 4.1).

Annual methane lifetime and sink trends in the 20th Century

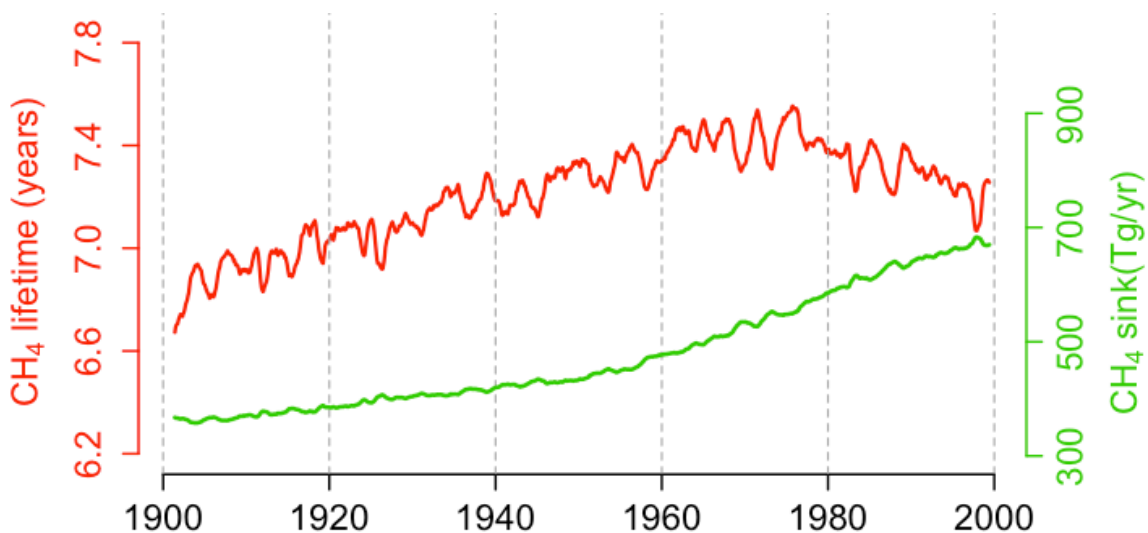


Figure 4.1 Annual atmospheric methane sinks (green) and methane lifetime (red) in the 1900-2000 period. Methane lifetime increases from 6.8 years to 7.2 years until 1970, then decreases by around 0.3 years in the last 30 years. Annual methane sinks (Tg/yr) increase overall in the target century. The rise in sinks is enhanced after 1960 as is the atmospheric methane mixing ratio.

The primary methane sink, by the “CH₄ + OH” reaction, varies spatially as well. Methane sinks are greater in the tropics and decrease with increasing latitude in both hemispheres. Figure 4.2 shows the sum of all “CH₄ + OH” rate in the troposphere spatially on the world map. The first panel (figure 4.2-A) shows the sum of all “CH₄ + OH” rate in 1901 and second panel (figure 4.2-B) of figure 4.2 shows the sum of all “CH₄ + OH” rate in 1999. There is a land-sea contrast in the methane sinks in the CCM-SOCOL.

In particular, over the tropical troposphere, the reaction rate increased with time. Over most of the regions in the tropics the reaction rate doubled during the 20th century.

Spatial distribution of methane sink by OH on the world map: 1901 & 1999

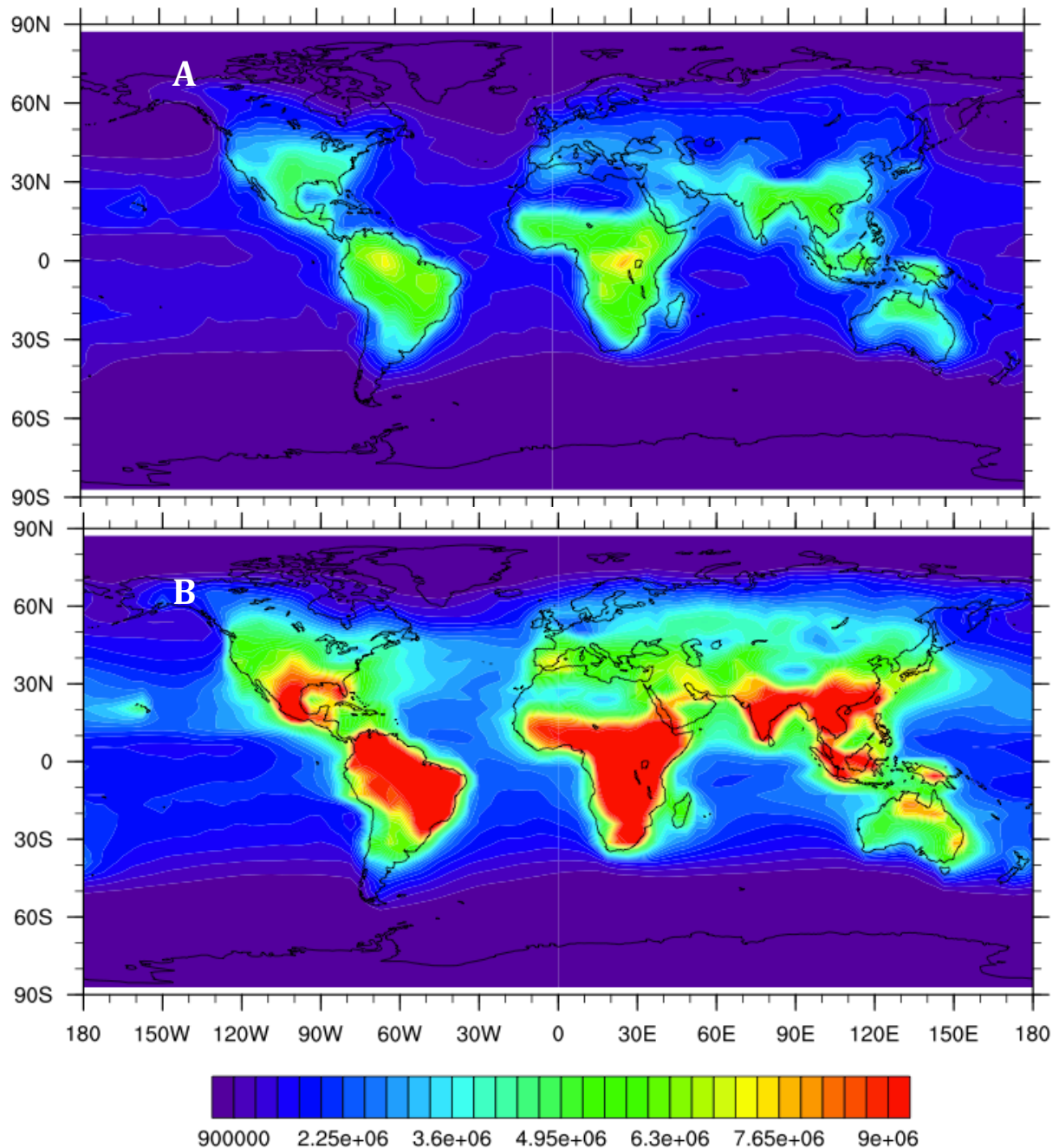


Figure 4.2 The annual sum of the "CH₄ + OH" reaction rate (molecules/cm³.sec) for the troposphere in 1901 (A) and 1999 (B) are given. The sum of the reaction rates increased globally and doubled over tropical regions. The OH causes a land-sea contrast in methane sinks, however the mixing ratio of methane is spatially uniform, i.e. it has the same prescribed concentration in all of the lowest model grids. At the beginning of the 20th Century (A), the Sahara and Middle-North Asia regions have similar methane destruction rates as neighboring marine regions (Tropical Section of the Atlantic). At the end (B), in both the Sahara and Middle-North Asia regions, methane destruction increases more than in neighboring marine regions. We also see a land-sea contrast in methane sinks over the troposphere of these regions, in 1999 this contrast extends into Europe and North America as well.

4.1. Methane Lifetime Results of The Sensitivity Runs

In order to analyze the cause of the increase in methane lifetime between 1900 and 1970, the fall in methane lifetime after 1970, and the missing VOCs and cloud impacts, sensitivity runs are used. The methane lifetimes calculated for the REF, as well as a modified version of the REF, CH₄_1901 and NO_x_CO_1951 runs are shown in figure 4.3.

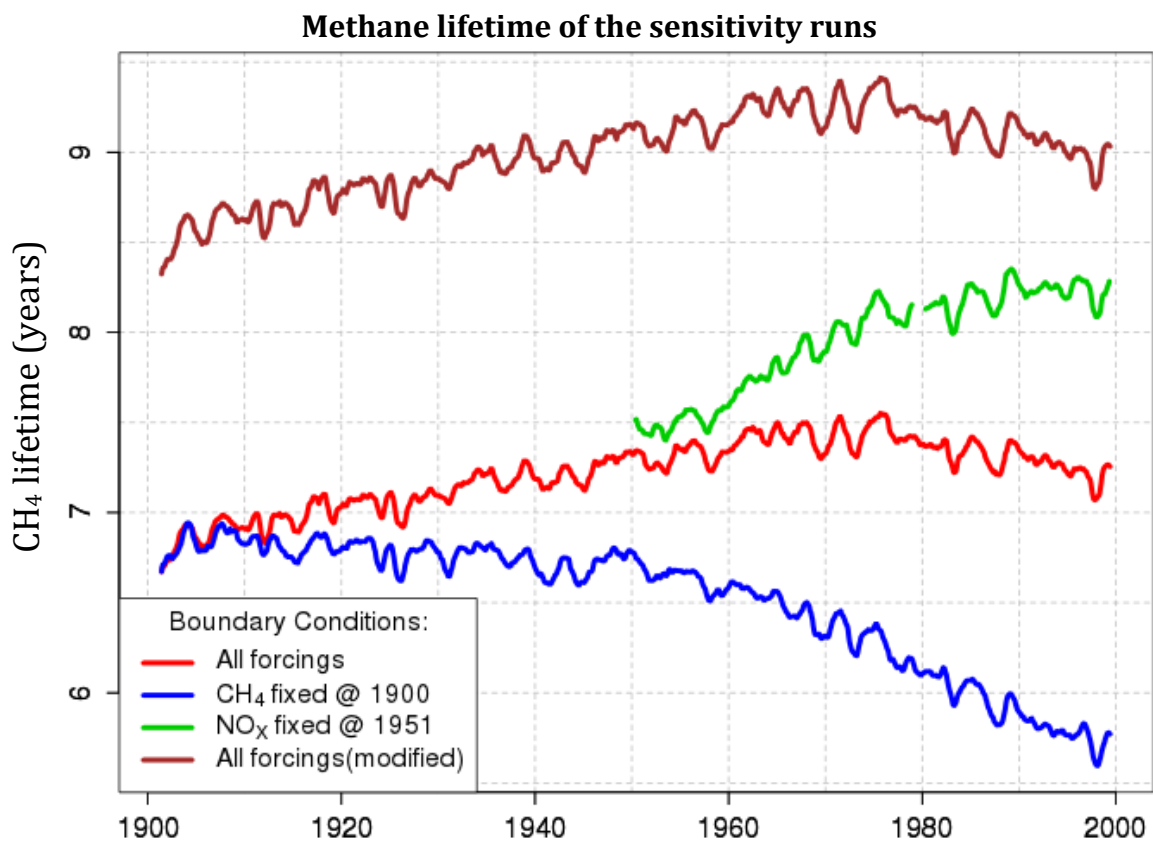


Figure 4.3 Methane lifetime, in monthly intervals, is shown for the REF run (red), CH₄_1901 run (blue), and NO_x_CO_1951 run (green). The modified REF run (brown) reflects missing VOC and cloud effects. In the REF run (red), methane lifetime increases from 6.8 to 7.4 years until the late 1970s, then decreases by about 0.3 years by the end of the century. In the NO_x_CO_1951 run (green), in which the NO_x mixing ratio is kept constant at 1951 levels, methane lifetime rises continuously. In CH₄_1901 (blue), methane lifetime decreases continuously and the fall is enhanced after 1960. Finally in the modified all forcings run (brown), the impact of VOCs and cloud parameterization on methane lifetime is modeled. The combined impact of VOCs and cloud parameterization leads to a reduction in OH levels by 20% globally. The methane lifetime pattern in the modified run is consistent with the REF run, however the methane lifetime varies, between 8.5 to 9.3 years, due to the reduction of OH.

Methane lifetime decreases by around 0.5 years from the beginning of the model simulation until 1960 in the CH₄_1901 run. The reduction then doubles and the calculated lifetime decreases by one year in the remaining 40 years of the model run. The increased reduction in methane lifetime after 1960 is similar to that seen in the REF run. However, in contrast to the CH₄_1901 and REF runs, methane lifetime rises

continuously, by about 0.8 years, in the NO_x_CO_1951 run and this rise is larger than in the REF run (figure 4.3).

Sensitivity runs help to understand the causes of the rise (1900-1960) and fall (after 1960) in methane lifetime shown by the red line in figure 4.3. The rise in methane lifetime in the first 60 years could be due to the rise in the methane mixing ratio. After 1950, tropospheric NO_x concentrations increase and there is a consequential rise in the NO_x mixing ratio in the troposphere, which results in increased O₃ formation. Thus, the rise in methane lifetime could stop due to the increase in OH, which is a consequence of the rising O(¹D) levels that result from ozone photolysis. This rising O(¹D) level could lead to an elevation of the “H₂O + O(¹D)” reaction, forming OH as a product. As a result, methane lifetime could be reduced after 1970.

The variability of methane lifetime in model studies is a further issue worth considering. The CCM SOCOL results show that methane lifetime is 7-7.5 years in the REF run and 8.5-9.3 years in the modified REF run in the 20th century (figure 4.3). In the study of Lelieveld et al. (1998) it is 7.9 for 1992, it is 8-9 years according to Prather et al. (2001) and 9.6 years in IPCC estimates (IPCC, 2001).

The failure to include the effects of clouds on photolysis rates and of VOC emissions on methane lifetimes are also important considerations. The lifetime, calculated for the modified version of SOCOL, is given in figure 4.3 (brown line). Andrea Stenke mimics VOCs in the model by implementing a condensed isoprene mechanism and a parameterized cloud effect on photolysis rates in SOCOL. In this modified version OH concentrations are reduced by 21.5% at 750 hPa and 15.3% at 250 hPa levels globally (Personal Communication). The global reduction in OH levels by 20% (in molecules/cm³) increased methane lifetime by about 1.7 years (8.5-9.3 years) due to a positive feedback mechanism.

4.2. Impact of the Changes in Tropospheric Temperature on Methane Oxidation

Rising tropospheric temperatures due to climate change could be the cause of the change in methane lifetime by affecting the “CH₄ + OH” reaction through the rate constant, “k”. The reaction rate of “CH₄ + OH” is calculated using the molecular densities of CH₄, OH and the rate constant, “k”, which is dependent on temperature:

$$k = 2.45 \times 10^{-12} \times e^{-1775/T} \quad (\text{eq.1})$$

The increase in tropospheric temperature could cause a rise in methane sinks and the diurnal temperature variability over the ocean and land could explain the land-sea contrast in sinks. Because temperature variability is an important factor, in order to quantify its impact on methane oxidation the “CH₄ + OH” reaction rate is calculated for selected regions of the land and marine troposphere with the help of sensitivity calculations (table 3.3).

In these scenarios; FX_CH4, FX_OH, and FX_Temp, the monthly mean reaction rates are calculated for different pressures (altitudes) in selected regions. The regions (table 3.2) are selected according to their atmospheric properties, including abundance of NO_x, CO, and ozone.

The reaction rates for the different scenarios are displayed in figure 4.4 for different altitudes over the ENSO region. The variability of the “CH₄ + OH” reaction rate is given for FX_CH4 (black line), FX_OH (red), FX_Temp (orange) and REF (blue). In FX_OH, the reaction rate is elevated by about 100% at the end of century, whereas in FX_CH4 it is reduced by about 50%. However, in FX_Temp, where the aim is to quantify the impact of temperature variability on methane destruction and lifetime, the reaction rate is reduced by about 1%.

From the plots in figure 4.4, we see that the increase in the tropospheric temperatures is only a minor contributor to the increase in methane sinks. Tropospheric temperature rise accounts for less than 1% of methane destruction in the ENSO 3.4 region and for around 1% in Europe and the Sahara. The effect of temperature through the reaction rate constant is not a major cause of the change in methane lifetime in the 20th century where the sinks are doubled and the methane lifetime rises by about 7% in the 1900-1975 period.

Sensitivity calculations for "CH₄ + OH" rate in ENSO 3.4 region

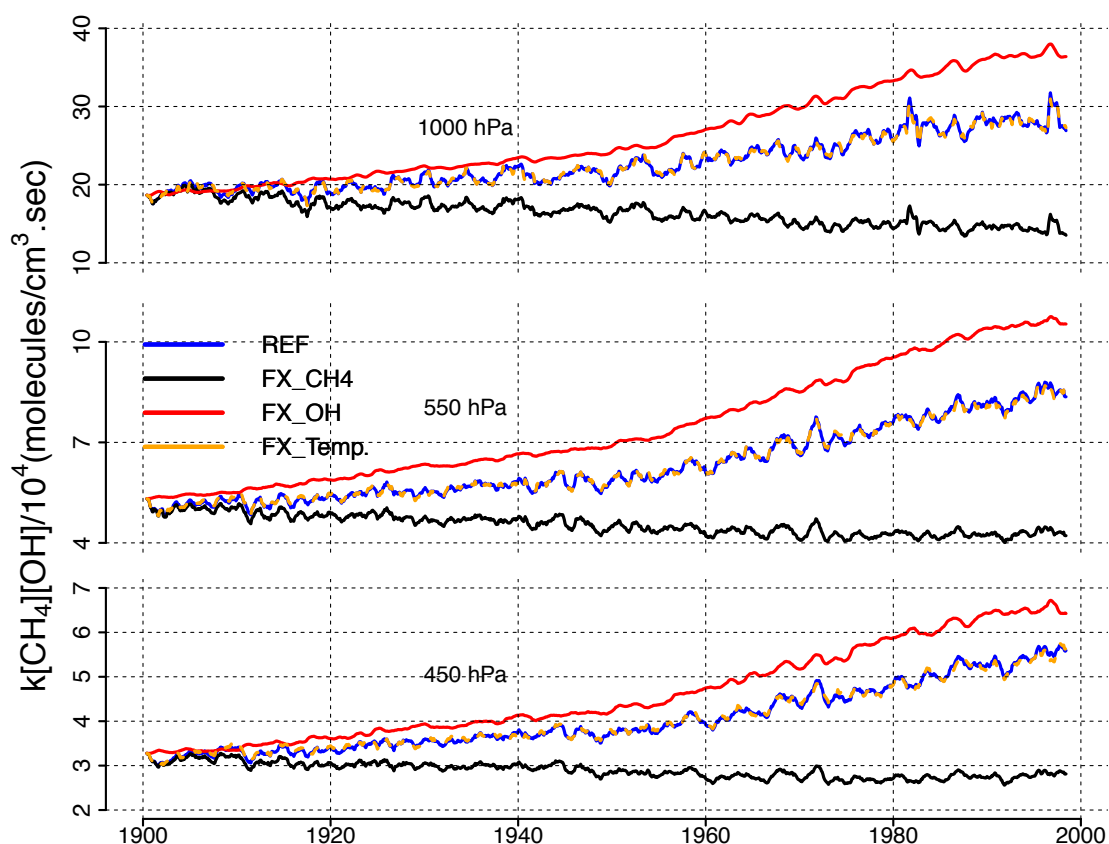


Figure 4.4 Changes in the calculated "CH₄ + OH" rate for the sensitivity calculations for a variety of pressures over the ENSO 3.4 region. At the panel on top, the mean "CH₄ + OH" reaction rate of REF (blue), FX_CH4 (black), FX_OH (red), FX_Temp (orange) is shown at 1000 hPa. In FX_CH4 (black), methane destruction follows the same pathway as the OH mixing ratio (figure 4.3). In FX_OH, methane destruction is dominated by the CH₄ mixing ratio and follows the CH₄ mixing ratio trend. Temperature variability due to climate change affects the "CH₄ + OH" reaction far less than the variability of OH and CH₄ mixing ratios. FX_temp trend (orange) has mostly the same pattern as the REF (blue).

The temperature rise due to climate variability and its impact on methane destruction both over land and ocean is approximately 1% in the target century. However, the methane destruction caused by the reaction methane undergoes with OH over land is much stronger than over the ocean (figure 4.2). Thus the likely impact of temperature change due to global warming on reaction rates is not significant and could not be responsible for the centennial change in methane lifetime in the 20th century.

4.3. Changes in the Mixing Ratio of Trace Gases in the 20th Century

The methane oxidation process is a chain of reactions that include other trace gases such as NO, NO₂, and O₃. It is also affected by the oxidation capacity of the atmosphere (the amount of HO_x, OH, etc.). Owing to the fact that the whole oxidation process is

determined by these components, it is important to know their variability and abundance during the target period as well.

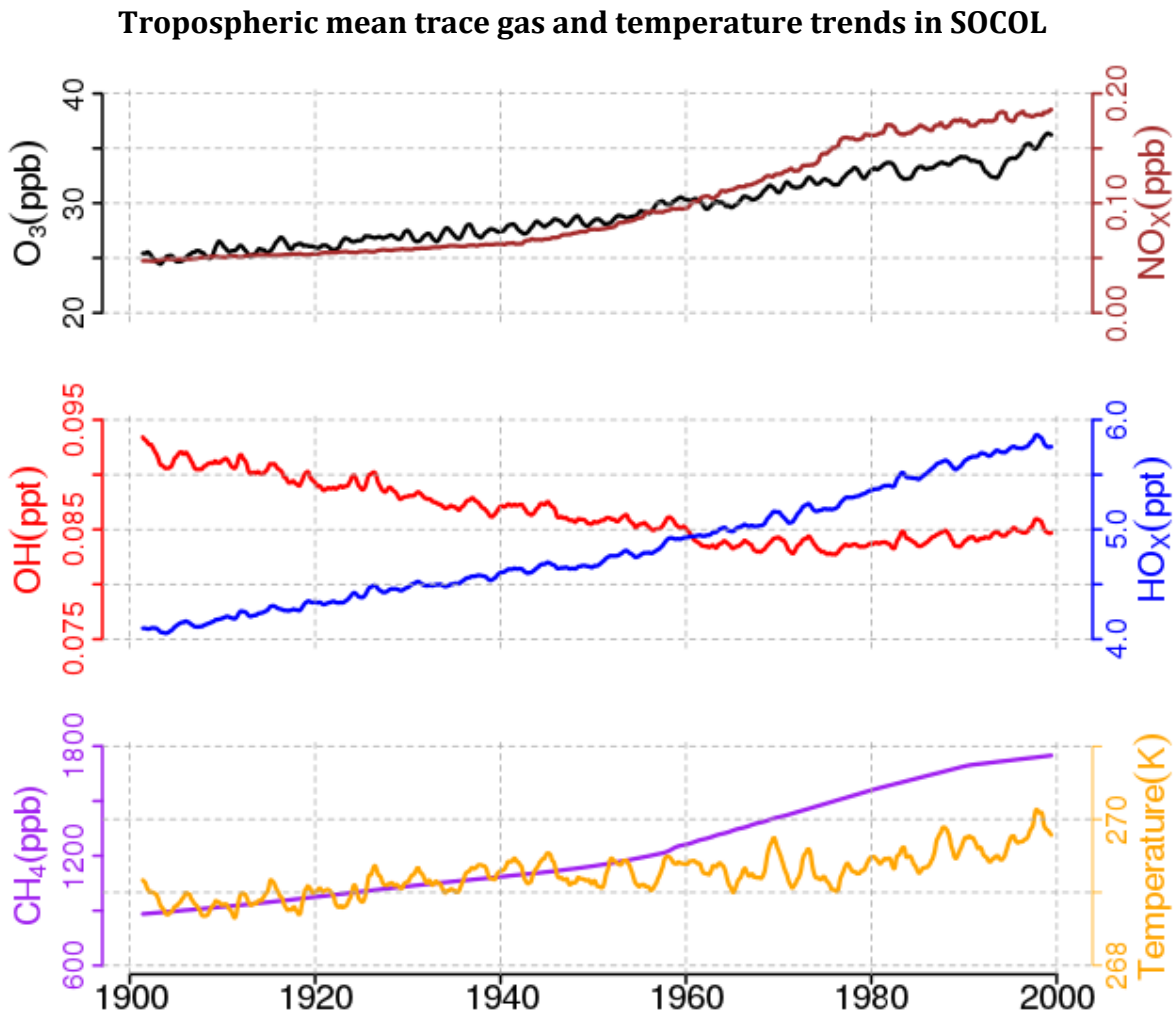


Figure 4.5 12-month moving average of tropospheric (mean of 1000-250 hPa levels);Ozone, NO_x, OH, HO_x, CH₄ and temperature in the CCM-SOCOL for the 1900-2000 period. Both tropospheric NO_x(brown) and ozone (black) rise in the 20th century. Increases in both substances become more significant during the second half of the century. Tropospheric ozone increased by 5 ppb_v during the first half of the century and increases by 11 ppb_v after 1950. The increase in tropospheric NO_x(brown) is about 200% higher during the second half of the century than in the 1900-1950 period. The increase in HO_x (blue), from 4 to 6 ppt_v, is mostly linear. The OH mixing ratio (red), decreases until the late 1960s, then stops and starts to increase in last 30 years, opposing the methane lifetime trend given in figure 4.1. The CH₄ mixing ratio rises by about 1000 ppb_v in the 20th century, mean tropospheric temperature increases by about 1^oK during the same period.

Mean ozone, HO_x and tropospheric temperatures have an increasing trend in the 1900-2000 period. The mean ozone mixing ratio increases by about 40% to 35 ppb at the end of the 20th century, from its initial level of 25 ppb at the beginning of the century. The increase in HO_x, similar to ozone, is about 40%. The mean tropospheric temperature, increases in the target period by about 1^oK, mostly after 1980 (figure 4.5).

Methane has an overall increasing trend; the rise approximately doubled after 1960. The NO_x mixing ratio rises with increasing emissions after the 1950s, however, increases in NO_x are lower after the 1980s due to the installation of catalytic converters, finally the mean mixing ratio reaches a level of 0.16 ppb (figure 4.5).

The main oxidizing agent for methane, OH, has a decreasing trend until 1960. At this point, the decrease in OH stops simultaneously with the rise in NO_x , and starts to increase until the end of the century.

4.4. Impact of Varying OH on Methane Lifetime

Variability in the concentration of OH radicals due to changes in its source or sink mechanisms may shed some light on the mechanism causing changes in methane lifetime, which first increases in the 1900 – 1960 period and then starts to decrease over the last 30 years. Since over 90% of atmospheric methane is removed by the reaction it undergoes with the OH.

4.4.1. Snapshot of the OH Sink by HNO_3 in the 20th Century

The reaction that OH undergoes with NO_2 is one of the major sinks of OH. Since OH is particularly important for changes in atmospheric methane, any shift in its sink could impact methane levels.

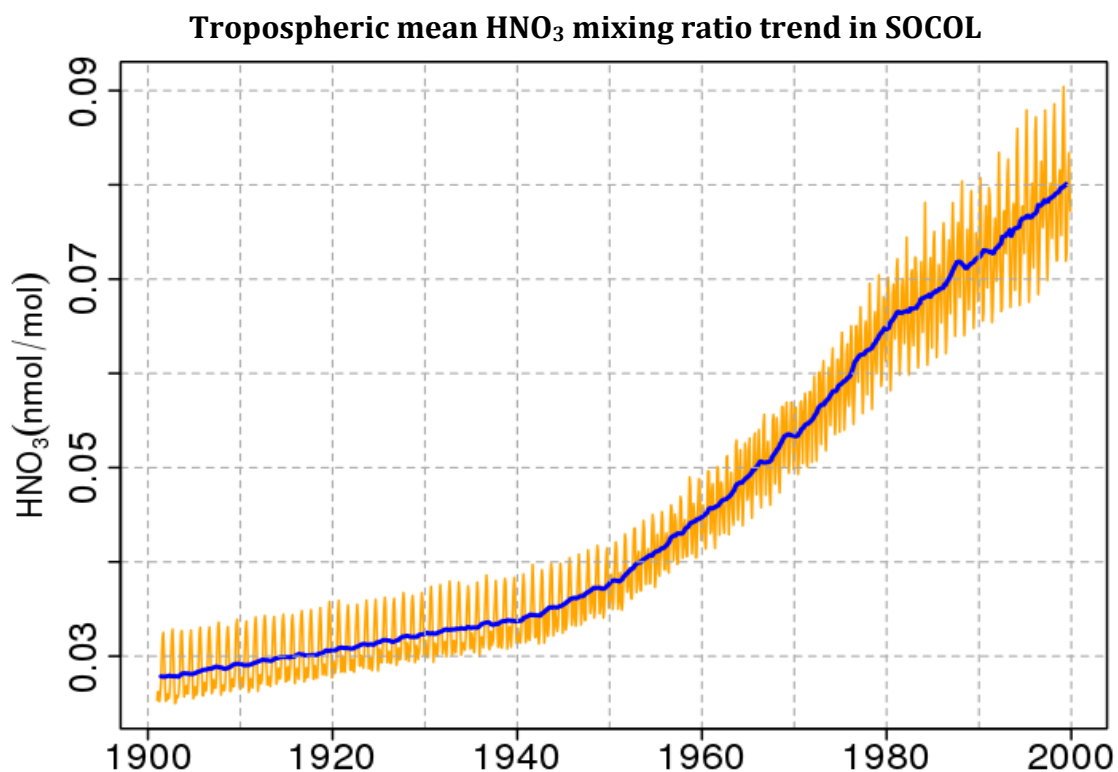


Figure 4.6 Monthly mean (orange line) and twelve-months moving average (blue line) of HNO_3 rises in the 20th century. Elevation in the tropospheric HNO_3 mixing ratio is enhanced after 1950 due to the increasing NO_x mixing ratio in the troposphere.

The OH sink, due to its reaction with NO_2 , increased in the 20th century with an enhanced growth after the 1960s (figure 4.6). By the start of the 1960s, HNO_3 formation increased along with the elevated NO_x mixing ratio in the troposphere (figure 4.5).

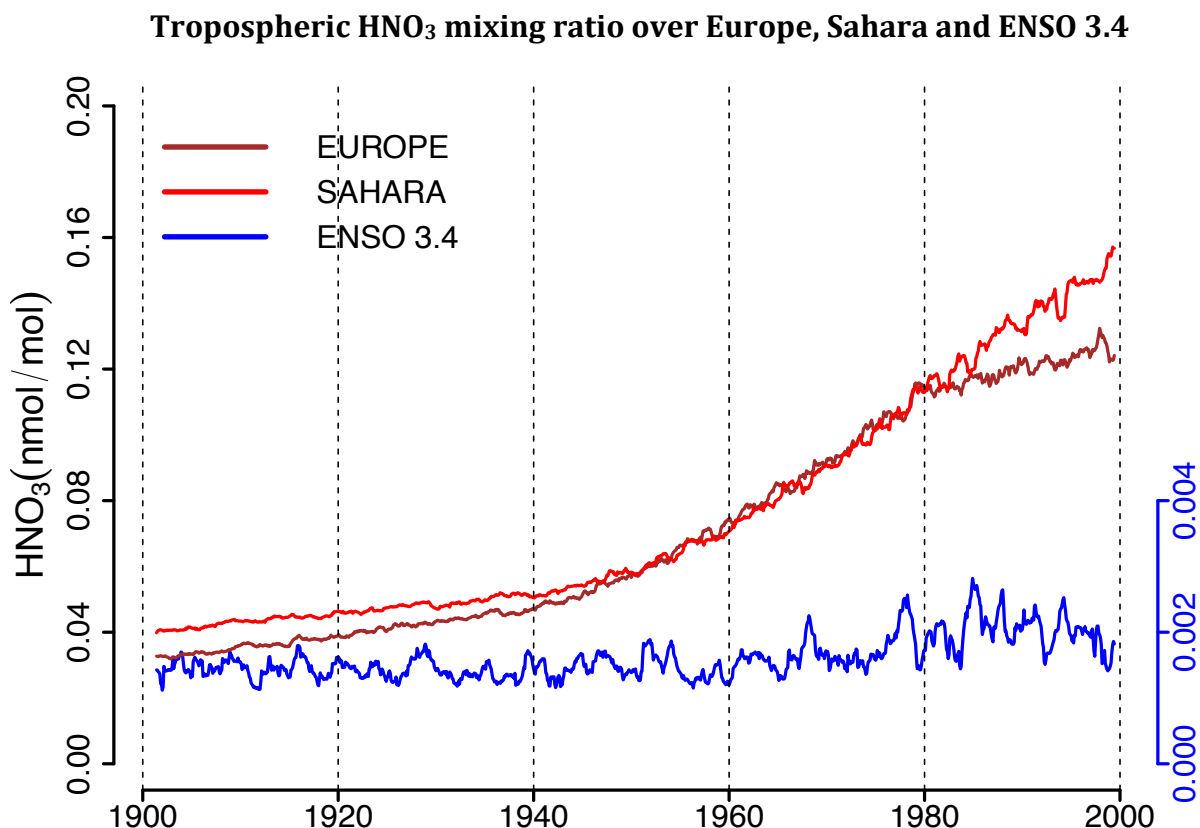


Figure 4.7 HNO_3 mixing ratio increases over Europe, the Sahara and the ENSO 3.4 region. The twelve-month moving average of the HNO_3 mixing ratio, sinks of OH by NO_2 , is given for surface level (1000 hPa) in Europe (brown, y-axis on left), the Sahara (red, y-axis on left) and the ENSO 3.4 region (blue, y-axis on right). Tropospheric HNO_3 elevation is higher over land in the Sahara and Europe, than in the marine ENSO 3.4 region, due to NO_x emissions.

The strength of the OH sink over the ENSO region is mostly constant in the 1900-2000 period. The OH sink is enhanced over land, by about 300% over the Sahara and about 200% over Europe, due to higher NO_x levels (figure 4.7).

The variation in OH sinks, as the primary cause for tropospheric methane variability, is considered as the main actor of methane destruction. A possible increase in OH sinks would lead to the consumption of OH and methane lifetime could be enhanced. However, the primary sink of OH, "OH + NO_2 ", is enhanced. Thus, the amount of HNO_3 formed increases, not only regionally (figure 4.7) but also globally (figure 4.6) in the

20th century. Moreover, HNO_3 formation is enhanced over land in Europe and the Sahara (figure 4.7). Elevated HNO_3 formation would have led to an increased methane lifetime through decreasing OH. Therefore, the variation in OH sinks by the reaction OH undergoes with NO_2 , is not responsible for the simulated long-term variability in OH and methane lifetime.

4.4.2. Snapshot of OH Mixing Ratio in the 20th Century

There is a strong exponential correlation between OH (ppt) and CH_4 lifetime (years) at the surface level (1000 mbars) in Europe (figure 4.8.a), the Sahara and the ENSO 3.4 region (figure 4.8.b). This strong correlation also exists at the remaining vertical levels.

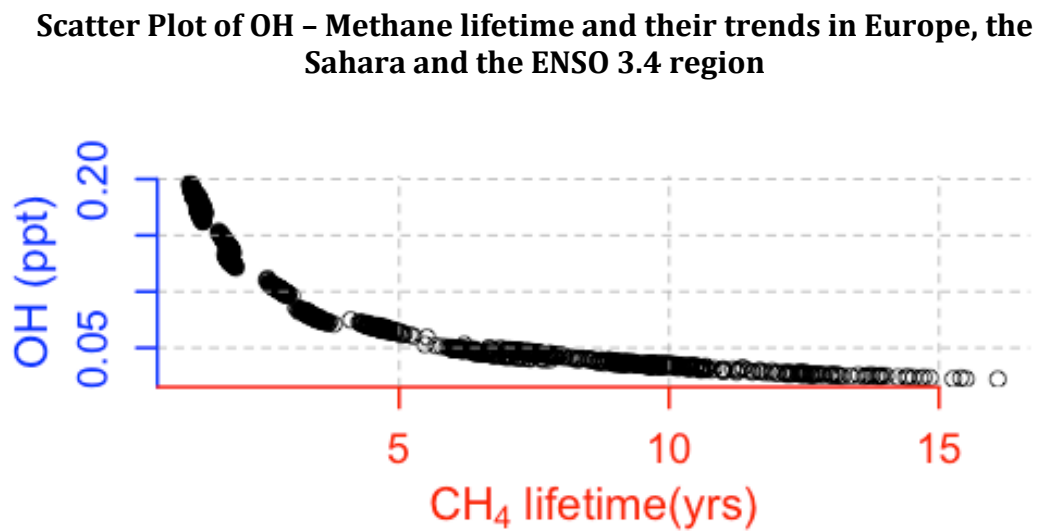


Figure 4.8.a Scatter plot of the mean methane lifetime and OH concentrations over Europe: Methane lifetime over Europe (1000-250 hPa) and Tropospheric OH mixing ratio (on Y-axis) are negatively correlated.

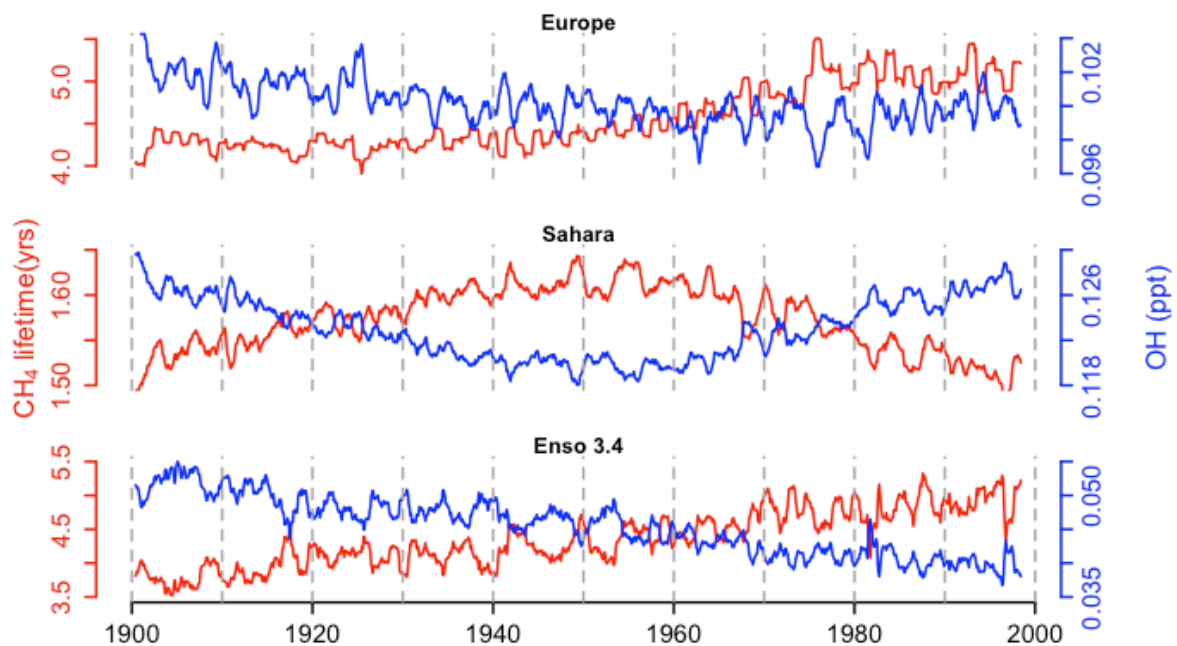


Figure 4.8.b CH₄ lifetime, OH mixing ratio and their correlation at surface level (1000 hPa) in Europe, the Sahara and the ENSO 3.4 Region: Methane lifetime (left y-axis) and OH mixing ratio (right y-axis) are given for the 20th century in the figure. Over Europe (top-panel), methane lifetime increases due to the decreasing OH mixing ratio until 1980. Then the elevation in methane lifetime stops like the decrease in OH mixing ratio in last 20 years due to the increase in the NO_x mixing ratio. Over the ENSO 3.4 region (lower-panel), methane lifetime rises over the entire period, meanwhile the OH mixing ratio is reduced. Over the Sahara, similar to Europe, methane lifetime falls until 1950, then rises back to the levels seen at the beginning of the century due to the increased transport of NO_x, ozone and H₂O.

In Europe, CH₄ lifetime increases until 1980 and then the rise slows and then halts. Simultaneously OH mixing ratio decreases until 1980 and this decrease stops by the end of the century (figure 4.8.b). The decadal variation in methane lifetime in Europe and the Sahara is due to changes in OH levels. NO_x emissions in Europe rise through to the end of the century along with the tropospheric ozone mixing ratio. The rise in ozone leads to an increase in O(¹D) which is the primary source of OH. Finally, the OH mixing ratio increases in the last 30 years of the model simulation, reducing methane lifetime in Europe.

Over the Sahara, CH₄ lifetime increases until the late 1950s at the surface level and then it falls to its 1900 level where OH mixing ratio, opposing CH₄ lifetime, decreases until the 1950s and then recovers to its initial level in 2000 (figure 4.8.b). Similar to the situation seen in Europe, OH levels increase in the Sahara after 1950. This elevation could be due to the transport of NO_x and ozone from neighboring land masses turning the Sahara into a NO_x-rich environment.

CH₄ lifetime, 3.5 years in 1900, increases to 5 years in 2000 in the ENSO 3.4 region (figure 4.8.b). The mixing ratio of OH is reduced by about 50% in the target period. The OH mixing ratio falls continuously in the ENSO 3.4 region since there are no surface NO_x sources and ozone transport is less than in Europe and the Sahara.

OH concentrations decrease until 1975, then their fall stops and starts to increase through to the end of the century. Since more than 90% of tropospheric methane is oxidized by OH, the decadal change of OH could be the cause for the variability in methane lifetime in the long-term. Methane lifetime, opposing OH, rises until 1975 and starts to decrease after 1975 (figure 4.9).

Mean tropospheric OH mixing ratio (ppt_v)

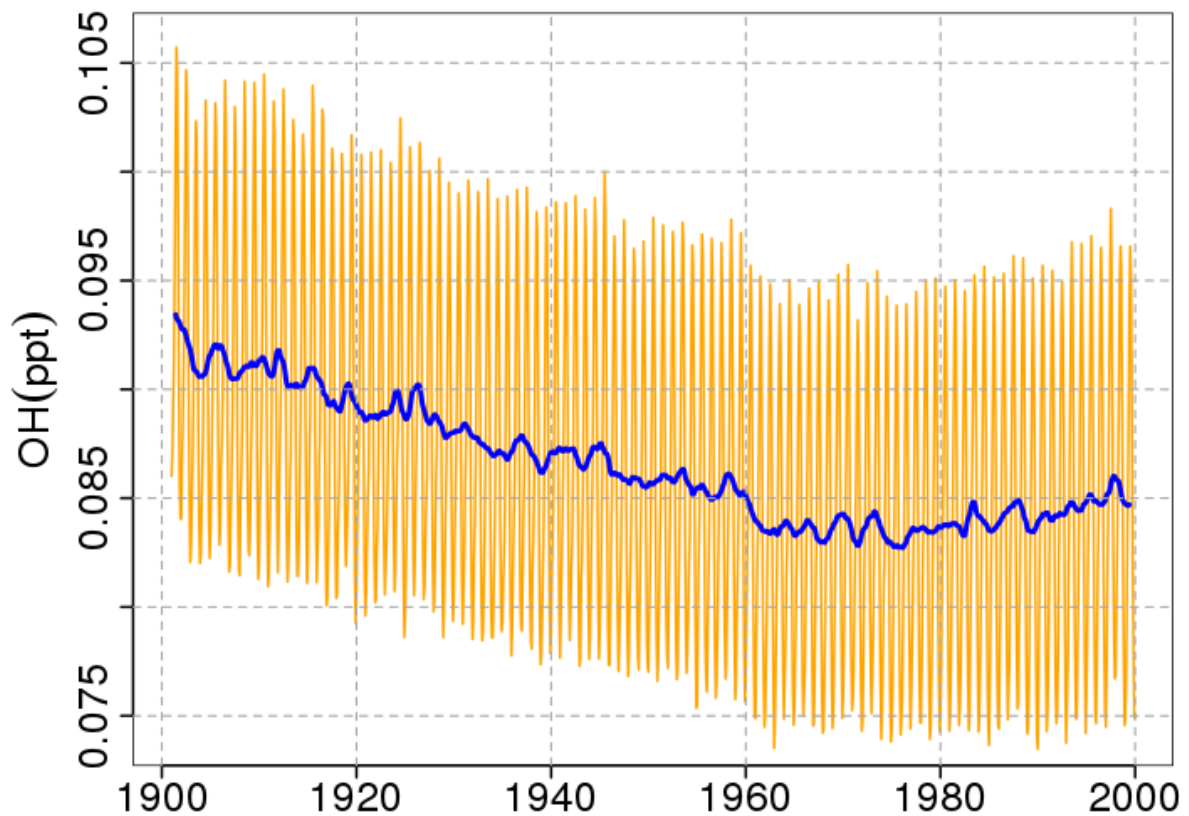


Figure 4.9 Monthly mean (orange) and twelve-month moving average (blue) OH levels in the troposphere for the 20th century. The OH mixing ratio has inter-annual and long-term variability. Due to the higher OH abundance in the northern hemisphere (NH), the monthly mean OH mixing ratio is highest globally during the NH summer when the OH mixing ratio reaches to its annual maximum level in the NH. Over the long-term, the OH mixing ratio goes down by around 12%. Then the fall in tropospheric OH levels stop and start to rise again in the last 20-25 years of the model simulation.

Mean OH molecular density is calculated for pressures ranging from 100 to 1000 hPa. OH levels in the SOCOL model are approximately 50% less compared to the reference study of Bousquet et al. (2005)

Molecular Density of OH in the CCM SOCOL

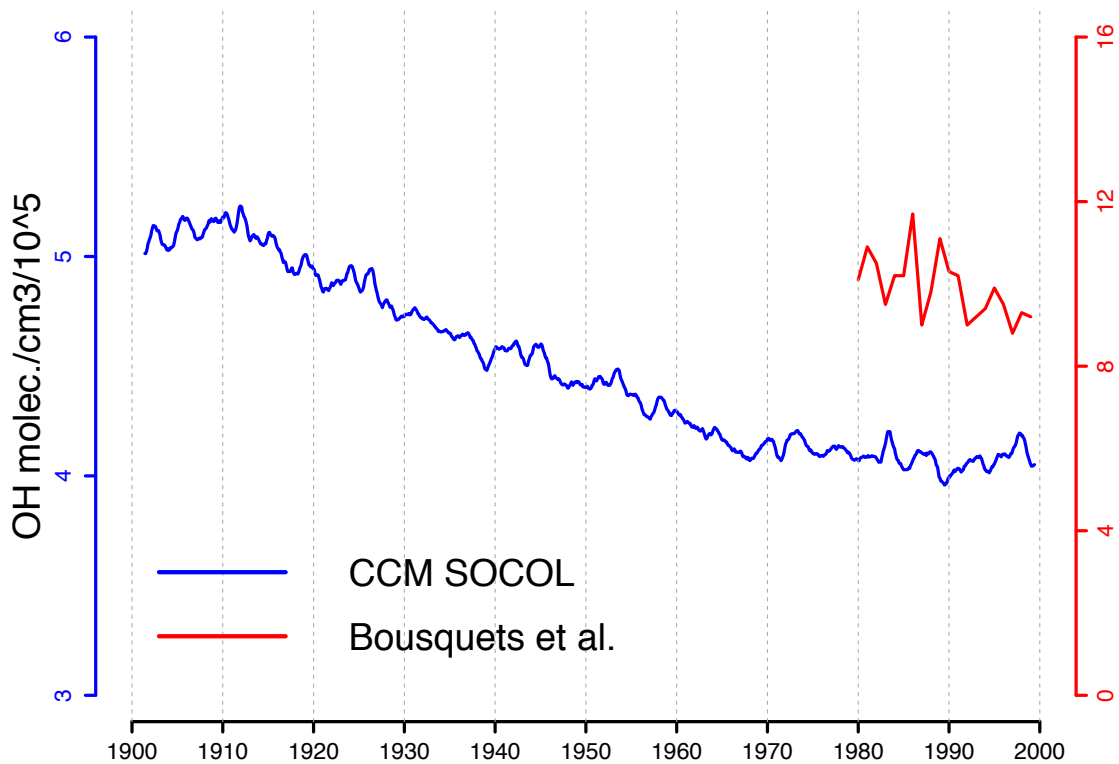


Figure 4.10 Mean molecular density of OH below 100 hPa in the CCM SOCOL and from the study by Bousquets et al., 2005. OH levels vary from 4-5.2 in the CCM SOCOL and from 8-12 molecules/cm³/10⁵ in the reference study.

4.4.3. Snapshot of O(¹D) Mixing Ratio in the 20th Century

The reaction of H₂O with O(¹D) is the primary source of OH. In this section, the variability of the O(¹D) mixing ratio in the CCM SOCOL is monitored to analyze its impact on the tropospheric mean OH. Ozone formation is enhanced by rising NO_x emissions in the 20th century. The increase in tropospheric ozone leads to increases in O(¹D). Thus, due to the reaction that O(¹D) undergoes with H₂O (R2), OH formation is enhanced.

In figure 4.11, the O(¹D) mixing ratios for 1000 and 450 hPa pressure layers of the model troposphere are given in the form of monthly means and 12-month averages. Over the continental troposphere, Europe and the Sahara, the O(¹D) mixing ratio increases by around 100% on an annual basis in the 20th century. In the ENSO 3.4 region the rise in O(¹D) is 40-50% during the same period, varying with altitude.

O(¹D) mixing ratio at 1000 and 450 hPa for Europe, the Sahara and the ENSO 3.4 region

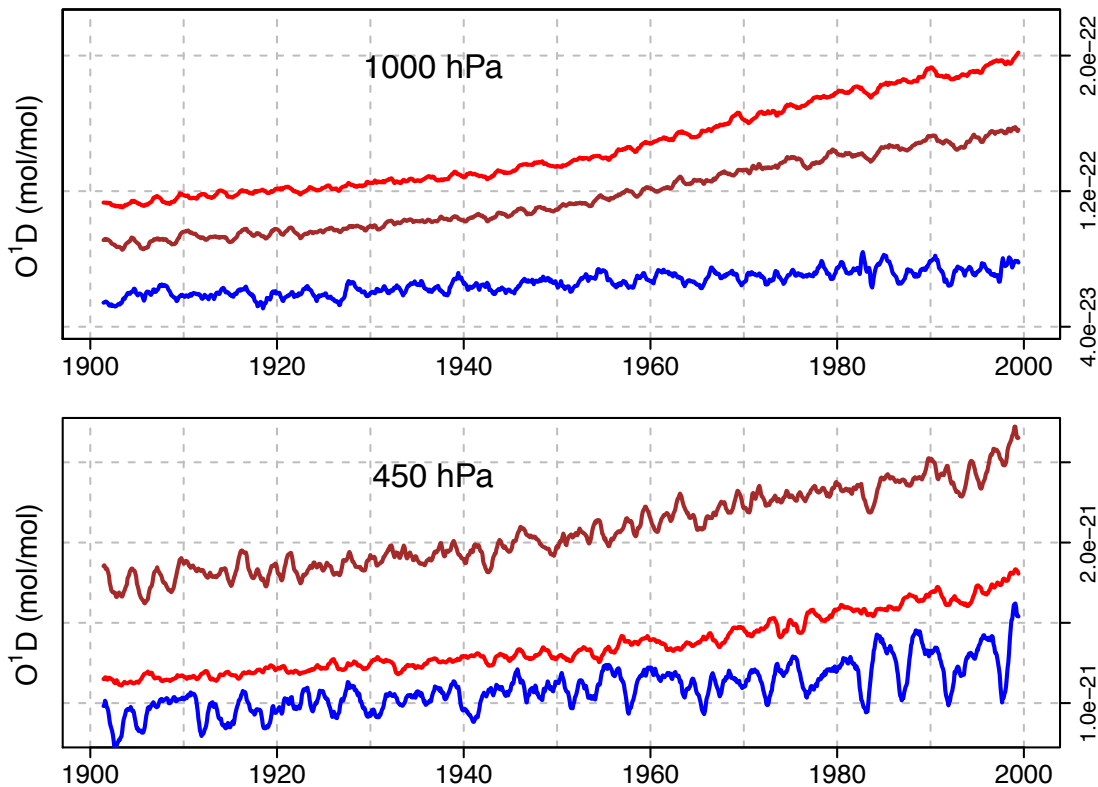


Figure 4.11 Twelve-month moving averages for O(¹D) mixing ratio over Europe (brown), the Sahara (red) and the ENSO (blue) regions for 450 and 1000 hPa. Tropospheric O(¹D) concentrations are higher over land than marine bodies.

Two other important mechanisms that impact OH abundance in the atmosphere are NO_x-rich (i) and (ii) NO_x-poor air conditions, partly producing or reducing OH. In order to monitor the impact of NO_x abundance on CH₄ destruction, the mean reaction rate of “HO₂ + O₃” and “HO₂ + NO” are calculated. These two reactions are particularly important to evaluate the strength of the CH₄ sink using two different mechanisms. Because in the NO_x-rich case(i), “HO₂ + NO” reaction leads to enhanced ozone production, whereas in the NO_x-poor case(ii), the “HO₂ + O₃” reaction reduces ozone during methane oxidation. In figure 4.11, the rates are given for Europe, the Sahara and the ENSO 3.4 regions to evaluate methane sink mechanisms in the troposphere over land and marine bodies.

Mean “HO₂ + O₃” and “HO₂ + NO” rates are calculated for Europe, the Sahara and the ENSO 3.4 region at the surface level (1000 hPa). Over Europe, both reaction rates are higher with respect to the Sahara and the ENSO regions due to the greater abundance of NO_x and ozone (figure 4.12). Higher “k[HO₂][NO]” implies that NO_x-rich conditions prevail and tropospheric ozone formation is enhanced as part of methane oxidation.

Over the Sahara the operating mechanism is similar to Europe. However, the difference between the rates is much higher than over the other regions of interest. The “HO₂ + NO” rate is about 6 times higher than “HO₂ + O₃”. The rise in both reaction rates is enhanced after the late 1950s as well (figure 4.12) due to increases in surface NO_x emissions.

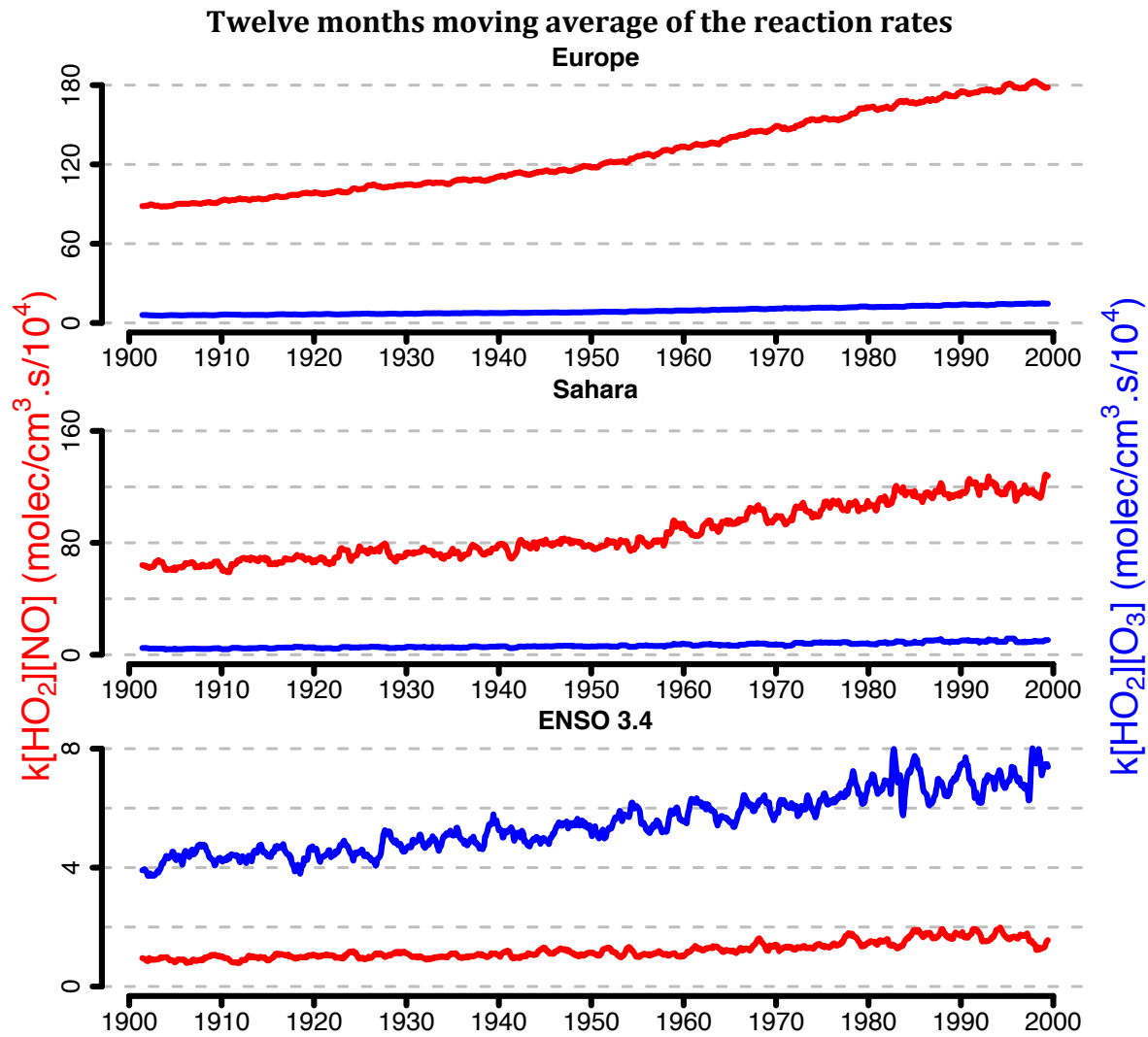


Figure 4.12 Mean reaction rates (molecules/cm³.sec/10⁴) of “HO₂ + O₃” (blue) and “HO₂ + NO” (red) at the surface level for Europe, the Sahara and the ENSO 3.4 region. The mean rate of “HO₂ + NO” is higher, by about 100 times, over land in the Sahara and Europe, due to higher NO levels. However in the marine troposphere, for example in the ENSO 3.4 region, the mean rate of “HO₂ + O₃” is about 6 times higher than the “HO₂ + NO” rate.

In the ENSO 3.4 region, opposing conditions prevail. The “HO₂ + O₃” rate is about 4 times higher than the “HO₂ + NO₂” rate. This implies that, due to lower NO_x abundance, ozone formation is less. Both ozone and NO_x are transported either from the stratosphere or neighboring land masses (figure 4.12).

Due to inter-hemispheric contrast, the contrast in tropospheric NO_x abundance, tropospheric ozone concentrations are higher in the northern hemisphere and are

increasing globally with rising NO_x emissions (figure 4.5). As a result, O(¹D) levels are elevated by ozone photolysis and this rise is greater over land where NO_x emissions are higher (figure 4.11).

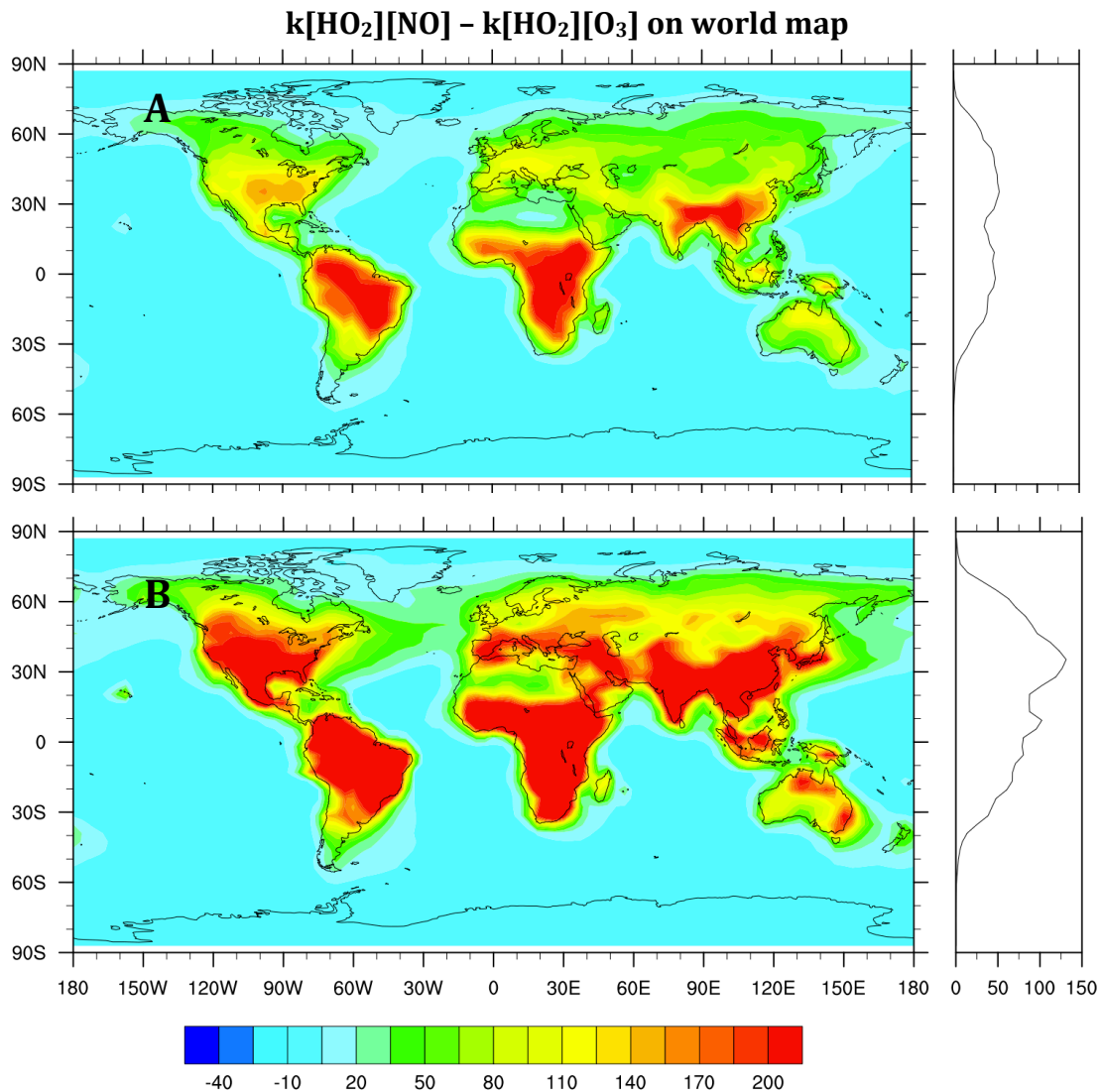


Figure 4.13 The spatial mean of “ $(k[\text{HO}_2][\text{NO}] - k[\text{HO}_2][\text{O}_3])/10^5$ ” on the world map (on the left) and the zonal mean “ $(k[\text{HO}_2][\text{NO}] - k[\text{HO}_2][\text{O}_3])/10^5$ ” (on the right) for 1901 (panel A) and 1999 (panel B). The difference between these rates is one of the surrogates used to analyze how methane is oxidized. A higher positive number implies ozone formation is a more likely consequence than ozone reduction. The higher positive numbers are calculated for land which are growing in time and extend to a wider spread spatially (panel A and B - on left). The zonal mean values of the mean rate differences indicate that the difference is higher in the northern hemisphere (NH) (panel B - on the right).

In order to monitor the areas where NO_x rich conditions are dominant, the mean difference between “HO₂ + NO” and “HO₂ + O₃” rates are calculated (figure 4.13). In panel A of figure 4.13, the mean difference in the rates (molecules/cm³.sec/10⁵) on the world map (left) and the zonal means on the vertical section on right are given for 1901. Similarly, the zonal mean difference in rates for 1999 is shown in panel B.

NO_x rich conditions become stronger in Middle Asia, especially over China and India, Europe, Northern America, Anatolia and the Middle East. Rising industrial and fossil fuel combustion are the primary causes of rising NO_x emissions (van Aardenne et al., 2001). This issue has been discussed by Lelieveld et al. (2009) and Smoydzin et al. (2012) for the Arabian Peninsula. Due to rising NO_x emissions and its resulting ozone transport, the Sahara partly evolved into a NO_x rich environment by the end of the century where NO_x induced methane oxidation prevails (figure 4.2-4.13) in 1901-1950 period.

According to the previous studies, the methane growth rate also has hemispheric dependence. The study of Spivakovsky et al. (2000) showed the inter-hemispheric difference in OH concentrations, which is particularly important for methane growth rates. The inter-hemispheric methane discrepancy could be caused by microbial activity (Kai et al., 2011) or source emissions (Aydin et al., 2011).

Mean reaction rates: Global, NH and SH

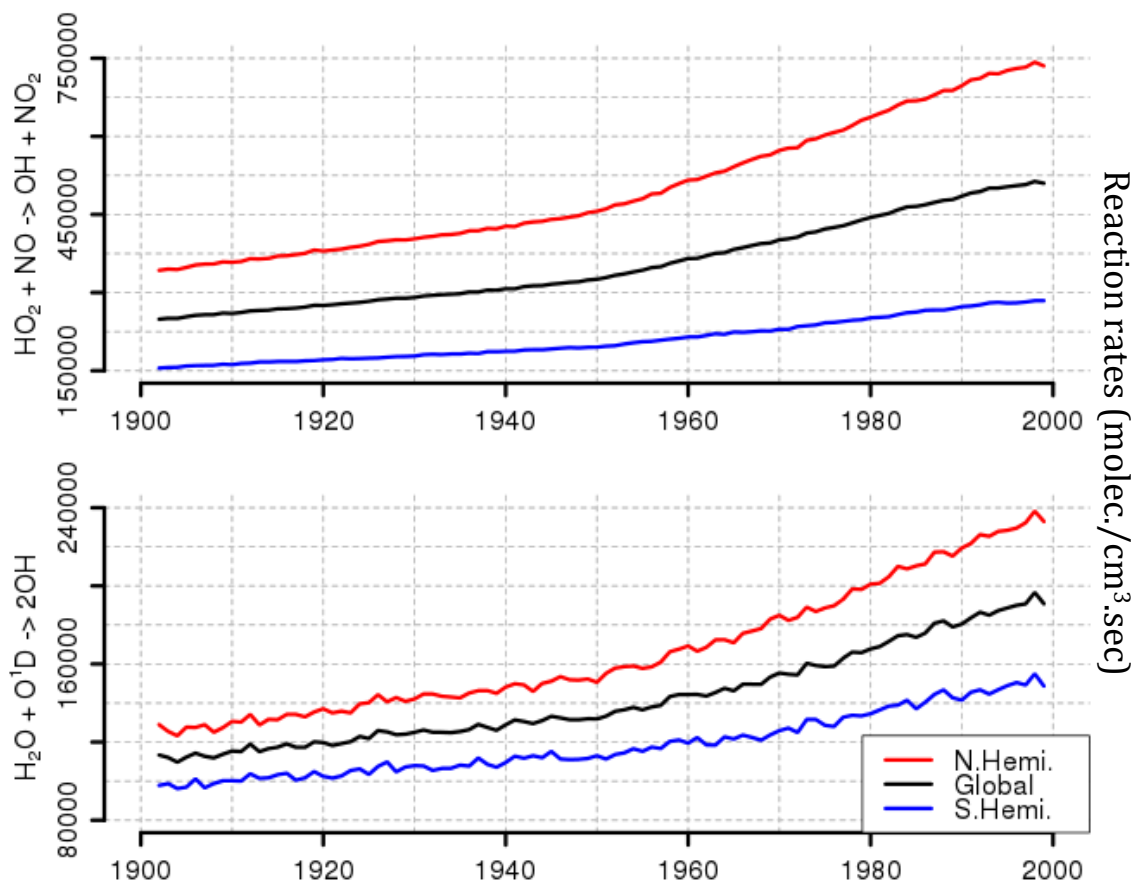


Figure 4.14 Global, Northern and Southern Hemispheric mean $k[\text{HO}_2][\text{NO}]$ and $k[\text{H}_2\text{O}][\text{O}(^1\text{D})]$ in $\text{molec./cm}^3 \cdot \text{sec}$. The rate of “ $\text{HO}_2 + \text{NO}$ ” reaction is higher in the Northern Hemisphere (NH). Due to higher abundance of $\text{O}(^1\text{D})$, the production of OH is higher in the NH. The rise in the “ $\text{H}_2\text{O} + \text{OH}$ ” rate after 1960 is about 100% higher in the NH as well.

Same discrepancies in OH levels are observed between the hemispheres, however methane concentrations are globally homogeneous in the modeled atmosphere. Global, Northern and Southern Hemispheric mean reaction rates of $k[\text{HO}_2][\text{NO}]$ and $k[\text{H}_2\text{O}][\text{O}^1\text{D}]$ are given in figure 4.14 for the 20th century. Both reactions occur at a higher frequency especially after 1950. Moreover, the rise in the rates is twice as large in the Northern Hemisphere due to the increasing NO_x and O_3 levels (figure 4.13-4.14). Consequently, globally increasing $k[\text{H}_2\text{O}][\text{O}^1\text{D}]$ is about 100% higher in the Northern Hemisphere when compared to the Southern Hemisphere (figure 4.14).

The model results imply that NO_x abundance and its variation is the cause of the methane lifetime alternation after 1960. Both methane emissions and the change in sink mechanisms are important to explain methane growth rate variability. The land-sea or the inter-hemispheric contrast in OH is due to the changing NO_x regime which determines methane lifetime.

5. CONCLUSIONS

The factors which are likely to determine the decadal change in methane lifetime and the land-sea contrast in methane sinks are investigated with the help of the CCM SOCOL. The variability of the determinants of methane sinks and its lifetime, including tropospheric temperature, methane sinks, and the oxidizing capacity of the atmosphere are monitored in the 20th century. The impacts of these determinants on methane sinks are analyzed for regions such as Europe, the Sahara and the ENSO 3.4 region, and for the whole troposphere. Our results imply that increasing NO_x abundance in the troposphere causes methane lifetime to decrease after 1960 (i) and the contrast in land-sea methane sinks (ii).

During the 1900-1960 period, methane enhances its own lifetime through an increasing methane mixing ratio. The amount of OH produced by the rising H₂O and O(¹D) levels is also lower than the OH amount that is reduced by the increasing methane mixing ratio during this period. Since methane itself is the dominant sink for OH in the atmosphere, the rising methane mixing ratio results in a reduction of OH by around 12% (figure 4.6).

After 1960, "H₂O + NO" and "O(¹D) + H₂O" reaction rates (figure 4.11, 4.13) and the fixed NO_x sensitivity run (figure 4.5) are addressing an additional increase in OH due to an increase in tropospheric ozone over the continental troposphere. Because of rising NO_x emissions, ozone formation is enhanced. This ozone enhancement produces an increase in the O(¹D) abundance in troposphere.

The "O(¹D) + H₂O" reaction, the primary source of OH, is enhanced with increasing O(¹D) availability (figure 4.10). This rise in the sources of OH lead to a reduced methane lifetime and growth rate by increasing the OH mixing ratio in the troposphere after 1960.

The impact of rising tropospheric temperatures on methane oxidation through the reaction rate constant, is analyzed with the help of sensitivity calculations. Mean tropospheric temperature rises by about 0.5°K in the 20th century (figure 4.3). This rise affects methane oxidation through the reaction rate constant ("CH₄ + OH" reaction) by an increase of 1%, however this rising temperature impact is not significant (figure 4.4).

There is a land-sea contrast in methane sinks even though the methane mixing ratio is spatially homogeneous in the CCM-SOCOL (figure 4.2). Because the tropospheric NO_x mixing ratio is higher over the land, especially in the northern hemisphere, ozone

formation is higher over the land. By the photolysis of ozone, more $O(^1D)$ is formed over land compared to marine bodies (figure 4.11). Increasing $O(^1D)$ levels lead to increased OH levels through the enhanced " $O(^1D) + H_2O$ " reaction. Since the NO_x mixing ratio is higher in the northern hemisphere, OH formation by the elevated $O(^1D)$ is higher in the northern hemisphere as well (figure 4.13).

This study focuses on the sinks of methane. Temperature change due to global warming is not the cause of the change in methane lifetime in CCM SOCOL. OH sinks are also not the cause since major sinks of OH, by methane and NO_2 , are increasing overall in the 20th century. Although the SOCOL model has deficiencies including its failure to include VOC emissions in the troposphere, to include the clouds direct impact on chemical reactions (not only through radiation), and prescribed methane concentrations that are spatially homogeneous, it demonstrates that NO_x emissions could play a significant role in determining methane lifetime which in turn affects atmospheric methane concentrations. This analysis could also imply that better OH estimates are required to accurately calculate methane lifetime.

6. ACKNOWLEDGEMENTS

I would like to express my deep gratitude to Professor Stefan Brönnimann and Professor Thomas Peter, my thesis supervisors, for their patient guidance, enthusiastic encouragement and useful critiques of this thesis work. I would also like to thank Dr. Stenke and Dr. Florian for their advice and assistance in data analysis. My grateful thanks are also extended to Mr. Ural for his help in scripting.

Finally, I wish to thank my parents and friends, especially to Mr. Mistik, Ms. Shariff and Ms. Baltacibasi, for their support and encouragement throughout my study.

BIBLIOGRAPHY

- Allan, W.**, et al.; Interannual variation of ^{13}C in tropospheric methane: Implications for a possible atomic chlorine sink in the marine boundary layer. *J. Geophys. Res.*, 110, D11306, doi:10.1029/2004JD005650. (2005)
- Aydin Murat**, Kristal R. Verhulst, Eric S. Saltzman, Mark O. Battle, Stephen A. Montzka, Donald R. Blake, Qi Tang & Michael J. Prather. Recent decreases in fossil-fuel emissions of ethane and methane derived from firn air. *Nature* 476, 198–201 (2011)
- Bekki, S.**, and K. S. **Law**, Sensitivity of the atmospheric CH_4 growth rate to global temperature changes observed from 1980–1982, *Tellus*, 49B, 409–416 (1997)
- Born, M.**, H. Dorr, and I. Levin.: Methane consumption in aerated soils of the temperate zone. *Tellus* , 42B, 2–8. (1990)
- Bousquet P.**, D. A. Hauglustaine, P. Peylin, C. Carouge, and P. Ciais, “Two decades of OH variability as inferred by an inversion of atmospheric transport and chemistry of methyl chloroform”, *Atmos. Chem. Phys.*, 5, 2635–2656, (2005)
- Brönnimann S.**, Eugster W., Wanner H., “Photo-oxidant chemistry in the polluted boundary layer under changing UV-B radiation”, *Atmospheric Environment*, 35, 3789 – 3797 (2001)
- Cagnazzo C.**, E. Manzini, M. A. Giorgetta, and P. M. De F. Forster, Impact of an improved radiation scheme in the MAECHAM5 General Circulation Model *Atmos. Chem. Phys. Discuss.*, 6, 11067–11092 (2006)
- Chen, G.**, D. Davis, J. Crawford, B. Heikes, D. O’Sullivan, M. Lee, F. Eisele, L. Mauldin, D. Tanner, J. Collins, J. Barrick, B. Anderson, D. Blake, J. Bradshaw, S. Sandholm, M. Carroll, G. Albercook, and A. Clarke, “An assessment of HO_x chemistry in the tropical Pacific boundary layer: comparison of model simulations with observations recorded during PEM tropics”, *J. Atmos. Chem.*, 38, 317–344 (2001)
- Cleveland R.B.**, W. S. Cleveland, J.E. McRae, and I. Terpenning. STL: A Seasonal-Trend Decomposition Procedure Based on Loess. *Journal of Official Statistics*, 6, 3–73. (1990)
- Dlugokencky E.J.**, Masarie K.A., Lang P.M. & Tans P.P. Continuing decline in the growth rate of the atmospheric methane burden. *Nature* 393, 447–450 (1998)
- Dlugokencky, E. J.**, Measurements of an anomalous global methane increase during 1998, *Geophys. Res. Lett.*, 28, 499–502 (2001)
- Egorova, T.**, Rozanov, E., Schlesinger, M. E., Andronova, N. G., Malyshev, S. L., Zubov, V., and Karol, I. L.: Assessment of the effect of the Montreal Protocol on atmospheric ozone, *Geophys. Res. Lett.*, 28, 2389–2392 (2001)
- Egorova, T.**, E. Rozanov, V. Zubov, and I. L. Karol: Model for Investigating Ozone Trends (MEZON), *Izvestiya, Atmospheric and Oceanic Physics*, 39, 277–292 (2003)
- EPA**, United States Environmental Protection Agency, “Methane and Nitrous Oxide Emissions from Natural Sources”, Office of Atmospheric Programs (6207) Washington, DC 20460, EPA 430-R-10-001, Chp. 1-1, April (2010)
- Etheridge, D. M.**, L. P. Steele, R. L. Langenfelds, R. J. Francey, J. M. Barnola and V. I. Morgan: Natural and anthropogenic changes in atmospheric CO_2 over the last 1000 years from air in Antarctic ice and firn, *Journal of Geophysical Research-Atmospheres*, 101,(D2), 4115–4128 (1996)
- Fiore M. Arlene**, Larry W. Horowitz, Edward J. Dlugokencky, and J. Jason West. Impact of meteorology and emissions on methane trends, 1990–2004. *GEOPHYSICAL RESEARCH LETTERS*, VOL. 33, L12809, doi:10.1029/2006GL026199 (2006)
- Fischer, A. M.**, M. Schraner, E. Rozanov, P. Kenzelmann, C. Schnadt Poberaj, D. Brunner, A. Lustenberger, B. P. Luo, G. E. Bodeker, T. Egorova, W. Schmutz, T. Peter, and S. Broennimann. Interannual-to-decadal variability of the stratosphere during the 20th century: ensemble simulations with a chemistry-climate model, *Atmos. Chem. Phys.*, 8, 7755–7777 (2008)
- Forster, P.**, V. Ramaswamy, P. Artaxo, T. Berntsen, R. Betts, D.W. Fahey, J. Haywood, J. Lean, D.C. Lowe, G. Myhre, J. Nganga, R. Prinn, G. Raga, M. Schulz and R. Van Dorland: Changes in Atmospheric Constituents and in Radiative Forcing. In: *Climate Change 2007: The Physical Science Basis. Contribution of Working Group I to the Fourth Assessment Report of the Intergovernmental Panel on Climate Change* [Solomon, S.,

- D. Qin, M. Manning, Z. Chen, M. Marquis, K.B. Averyt, M.Tignor and H.L. Miller (eds.)). Cambridge University Press, Cambridge, United Kingdom and New York, NY, USA. (2007)
- Fung**, I., J. John, J. Lerner, E. Matthews, M. Prather, L.P. Steele and P.J. Fraser: Three-dimensional model synthesis of the global methane cycle. *J. Geophys. Res.*, 96, 13033-13065. (1991)
- Goldewijk**, K. K.: Estimating global land use change over the past 300 years: The HYDE Database, *Global Biogeochemical Cycles*, 15,(2), 417-433 (2001)
- Hein**, R., P.J. Crutzen and M. Heinmann: An inverse modeling approach to investigate the global atmospheric methane cycle. *Global Biogeochem. Cycles*, 11, 43-76. (1997)
- Hoyle**, C. R.: Three dimensional chemical transport model study of ozone and related gases 1960–2000, Eidgenossische Technische Hochschule, Zürich, Dissertation No. 16271 (2005)
- IPCC**, Summary for Policymakers. In: *Climate Change 2007: The Physical Science Basis. Contribution of Working Group I to the Fourth Assessment Report of the Intergovernmental Panel on Climate Change* [Solomon, S., D. Qin, M. Manning, Z. Chen, M. Marquis, K.B. Averyt, M.Tignor and H.L. Miller (eds.)]. Cambridge University Press, Cambridge, United Kingdom and New York, NY, USA. (2007)
- Johnson** C. E., W. J. Collins, D. S. Stevenson, and R. G. Derwent, Relative roles of climate and emissions changes on future tropospheric oxidant concentrations, *J. Geophys. Res.*, 104, 18,631–18,645 (1999)
- Johnson** C. E., D. S. Stevenson, W. J. Collins, and R. G. Derwent, Role of climate feedback on methane and ozone studied with acoupled Ocean- Atmosphere-Chemistry model, *Geophys. Res. Lett.*, 28, 1723–1726 (2001)
- Johnson** C.E., D. S. Stevenson,1 W. J. Collins, and R. G. Derwent. Interannual variability in methane growth rate simulated with a coupled Ocean-Atmosphere-Chemistry model. *GEOPHYSICAL RESEARCH LETTERS*, VOL. 29, NO. 19, 1903, doi:10.1029/2002GL015269 (2002)
- Kai** Fuu Ming, Stanley C. Tyler, James T. Randerson1 & Donald R. Blake Reduced methane growth rate explained by decreased Northern Hemisphere microbial sources, 194, *Nature*, Vol 476, doi:10.1038/nature10259 (2011)
- Karlsdottir**, S., and I. S. A. Isaksen, “Changing methane lifetime: Possible cause for reduced growth”, *Geophys. Res. Lett.*, 27, 93–96 (2000)
- Khalil**, M. A. K., and R. A. Rasmussen, Interannual variability of atmospheric methane: possible effects of the El Niño-Southern Oscillation, *Science*, 232, 56–58 (1986)
- Lelieveld**, J., Paul J. Crutzen and Frank J. Dentener. Changing concentration, lifetime and climate forcing of atmospheric methane *Tellus*, 50B, 128–150 (1998)
- Lelieveld**, J., Hoor, P., Joöckel, P., Pozzer, A., Hadjinicolaou, P., Cammas, J.-P., and Beirle, S.: Severe ozone air pollution in the Persian Gulf region, *Atmos. Chem. Phys.*, 9, 1393–1406, doi:10.5194/acp-9-1393-2009, 6332, 6333, 6335, 6345 (2009)
- Manzini**, E. and L. **Bengtsson**: Stratospheric climate and variability from a general circulation model and observations, *Clim. Dyn.*, 12, 615–639 (1996)
- Neue** H., “Methane emission from rice fields: Wetland rice fields may make a major contribution to global warming”. *BioScience*, 43 (7), 466-73 (1993)
- Penkett**, S. A., Monks, P. S., Carpenter, L. J., Clemitshaw, K. C., Ayers, G. P., Gillett, R. W., Galbally, I. E., and Meyer, C. P. “Relationship between ozone photolysis rates and peroxy radical concentrations in clean marine air over the Southern Ocean”, *J. Geophys. Res.-Atmos.*, 102, 12805–12817 (1997)
- Platt**, U., W. Allan, and D.C. Lowe: Hemispheric average Cl atom concentration from 13C/12C ratios in atmospheric methane. *Atmos. Chem. Phys.*, 4, 2393–2399.(2004)
- Prather** Micheal J. Lifetimes and time scales in atmospheric chemistry *Phil. Trans. R. Soc. A* 2007 365, 1705-1726 doi: 10.1098/rsta.2007.2040 (2007)
- Rayner**, N. A., D. E. Parker, E. B. Horton, C. K. Folland, L. V. Alexander, D. P. Rowell, E. C. Kent and A. Kaplan: Global analyses of sea surface temperature, sea ice, and night marine air temperature since the late nineteenth century, *Journal of Geophysical Research-Atmospheres*, 108,(D14), 4407 (2003)
- Roeckner**, E., Arpe, K., Bengtsson, L., Christoph, M., Claussen, M., Du`menil, L., Esch, M., Giorgetta, M., Schlese, U., and Schulzweida, U.: The atmospheric general circulation model ECHAM4: Model description

and simulation of the present-day climate, Max-Planck-Institut für Meteorologie, Hamburg, Report No. 218 (1996)

Rozanov, E., Schlesinger, M. E., Zubov, V., Yang, F., and Andronova, N. G.: The UIUC three-dimensional stratospheric chemical transport model: Description and evaluation of the simulated source gases and ozone, *J. Geophys. Res.*, 104, 11 755– 11 781 (1999)

Rozanov, E., Schlesinger, M. E., and Zubov, V.: The University of Illinois, Urbana-Champaign three-dimensional stratosphere-troposphere general circulation model with interactive ozone photochemistry: Fifteen-year control run climatology, *J. Geophys. Res.*, 106, 27 233–27 254 (2001)

Schmitt, A., and B. Brunner, Emissions from aviation and their development over time, Pollutants from air traffic – results of atmospheric research 1992–1997, DLR Mitt. 97-04, edited by: Schumann, U., Chlond, A., Ebel, A., Kärcher, B., Pate, H., Schlager, H., Schmitt, A., and Wendling, P., 37-52, DLR Köln, Germany. (1997)

Schultz, M.G, A. Heil, J.J. Hoelzemann, A. Spessa, K. Thonicke, J. Goldammer, A.C. Held, J.M. Pereira, Global Emissions from Wildland Fires from 1960 to 2000, submitted to *Global Biogeochem. Cycles* (2007)

Schraner M.,E. Rozanov, C. Schnadt Poberaj, P. Kenzelmann, A. M. Fischer, V. Zubov, B. P. Luo, C. R. Hoyle, T. Egorova, S. Fueglistaler, S. Broennimann, W. Schmutz, and T. Peter. Technical Note: Chemistry-climate model SOCOL: version 2.0 with improved transport and chemistry/microphysics schemes. *Atmos. Chem. Phys.*, 8, 5957-5974 (2008)

Smoydzin L., M. Fnais, and J. Lelieveld, Ozone pollution over the Arabian Gulf – role of meteorological conditions, *Atmos. Chem. Phys. Discuss.*, 12, 6331–6361, doi:10.5194/acpd-12-6331-2012. (2012)

Spivakovsky C. M., J. A. Logan, S. A. Montzka, Y. J. Balkanski, M. Foreman-Fowler, D. B. A. Jones, L. W. Horowitz, A. C. Fusco, C. A. M. Brenninkmeijer, M. J. Prather, S. C. Wofsy, and M.B. McElroy. Three-dimensional climatological distribution of tropospheric OH' Update and evaluation. *JOURNAL OF GEOPHYSICAL RESEARCH*, VOL. 105, NO. D7, PAGES 8931-8980, APRIL 16 (2000)

Taraborelli D., M. G. Lawrence, J. N. Crowley, T. J. Dillon, S. Gromov, C. B. M. Groß, L. Vereecken & J. Lelieveld. Hydroxyl radical buffered by isoprene oxidation over tropical forests. *Nature Geosciences*, 5, 190–193 (2012)

Trenberth, Kevin E., David P. **Stepaniak**: Indices of El Niño Evolution. *J. Climate*, 14, 1697–1701 (2001)

Whalley L. K., K. L. Furneaux, A. Goddard, J. D. Lee, A. Mahajan, H. Oetjen, K. A. Read, N. Kaaden, L. J. Carpenter, A. C. Lewis, J. M. C. Plane, E. S. Saltzman, A. Wiedensohler, and D. E. Heard. The chemistry of OH and HO₂ radicals in the boundary layer over the tropical Atlantic Ocean. *Atmos. Chem. Phys.*, 10, 1555–1576 (2010)

WMO: Scientific assessment of ozone depletion: 2002, Global ozone research and monitoring project, No. 47, (World Meteorological Organization), Geneva. (2003)

WMO, World Meteorological Organization, “*Twenty questions and answers about the ozone layer: 2006 update. Scientific assessment of ozone depletion: 2006*”, available on: <http://www.esrl.noaa.gov/csd/assessments/ozone/2006/twentyquestions.html> (6 May, 2011) (2006)

van Aardenne, J. A., F. J. Dentener, J. G. J. Olivier, C. G. M. K. Goldewijk and J. Lelieveld: A 1 degrees x 1 degrees resolution data set of historical anthropogenic trace gas emissions for the period 1890-1990, *Global Biogeochemical Cycles*, 15,(4), 909-928 (2001)

Declaration

under Art. 28 Para. 2 RSL 05

Last, first name: KILIC, DOGUSHAN

Matriculation number: 10-115-582

Programme: Climate Sciences

Bachelor

Master

Dissertation

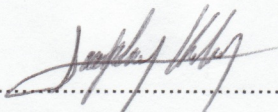
Thesis title: The Determinants of Decadal
methane Lifetime Change in Chemistry
Climate Model SOCOL: 1900-2000

Thesis supervisor: Prof. Stefan Brönnimann

I hereby declare that this submission is my own work and that, to the best of my knowledge and belief, it contains no material previously published or written by another person, except where due acknowledgement has been made in the text. In accordance with academic rules and ethical conduct, I have fully cited and referenced all material and results that are not original to this work. I am well aware of the fact that, on the basis of Article 36 Paragraph 1 Letter o of the University Law of 5 September 1996, the Senate is entitled to deny the title awarded on the basis of this work if proven otherwise.

..... Bern, 20/11/2012

Place, date

..... 

Signature